Natural Resources Canada | Ressources naturelles Canada

GEOLOGICAL SURVEY OF CANADA
OPEN FILE 8934

Seismic hazard investigations at select DND facilities in southwestern British Columbia: subduction, in-slab, and crustal scenarios

C. Paul and J.F Cassidy

2022

Canada

ISSN 2816-7155
ISBN 978-0-660-46255-4
Catalogue No. M183-2/8934E-PDF

GEOLOGICAL SURVEY OF CANADA
OPEN FILE 8934

Seismic hazard investigations at select DND facilities in southwestern British Columbia: subduction, in-slab, and crustal scenarios

C. Paul and J.F Cassidy

2022

Permanent link: https://doi.org/10.4095/331199

This publication is available for free download through GEOSCAN (https://geoscan.nrcan.gc.ca/).

Recommended citation

Paul, C. and Cassidy, J.F., 2022. Seismic hazard investigations at select DND facilities in southwestern British Columbia: subduction, in-slab, and crustal scenarios; Geological Survey of Canada, Open File 8934, 1 .zip file. https://doi.org/10.4095/331199

Publications in this series have not been edited; they are released as submitted by the author

Contents

Figures

1 ACKNOWLEDGEMENTS

We would like to thank the Department of National Defence for making this research possible. We would also like to thank Tiegan Hobbs and Defence Research and Development Canada – Centre for Operation Research and Analysis (DRDC CORA) for providing data and guidance used throughout this research. Additionally, we thank Tiegan Hobbs for her careful reviewing and helpful comments.

2 ABSTRACT

Southwest British Columbia has some of the highest seismic hazard in Canada and is home to facilities owned by the Department of National Defence which support operations on the west coast of the country. We investigated the potential impact of seismic hazards on these government facilities. The hazard is from three primary seismic sources: subduction interface, crustal and in-slab earthquakes. In consultation with DRDC, we have produced representative earthquake scenarios for each source. The subduction scenario we constructed was a moment magnitude (M_w) 8.9 earthquake extending along the entire Cascadia Subduction Zone from 4 to 18 km depth. We created an M_w 6.8 earthquake occurring along a 30 km fault at between 52 and 60 km depth below Boundary Bay to represent in-slab events. The final scenario, representing a crustal source, was an M_w 6.4 along the central 47 km of the Leech River Valley-Devil's Mountain Fault system. The Cascadia subduction scenario dominated the shaking hazard over much of the study region. Meanwhile, the in-slab and crustal scenarios have higher, more localized hazards in Vancouver and Victoria. In addition to the primary ground motion hazard, we also examined secondary seismic hazards: secondary amplification effects, landslides, liquefaction, surface ruptures, tsunami, flooding, fire, and aftershocks. Each of the secondary hazards had varying impacts depending on the scenario and locations within the region.

3 PREFACE

This document is an overview of the scenario earthquakes and their expected hazards as designed by Natural Resources Canada (NRCan), and Defence Research and Development Canada – Centre for Operation Research and Analysis (DRDC CORA). These scenarios were constructed to represent specific types of events but are purely hypothetical. This study is not a prediction that these events will occur as presented here but are designed to be useful for planning purposes.

We calculated the hazard estimates shown here using modelling techniques based on the current knowledge of earthquake engineering and science. In any earthquake modelling process, there are epistemic uncertainties to any inputs and aleatory variability in the processes. Therefore, these results should only be used as a guide to the types of potential outcomes of an earthquake and not considered as the exact expected outcome of a major event in Southwestern British Columbia.

This article documents the seismic hazard assessment, including secondary effects. A companion paper provides the earthquake risk and impacts analyses.

4 INTRODUCTION

4.1 REGION

Southwestern British Columbia (SWBC) has a population of 3.5 million people and includes the most populated regions of British Columbia: Greater Vancouver (~2.46 million people), Capital Regional District (CRD) (~383 000), Fraser Valley (~296 000), and Nanaimo (~156 000) (Statistics Canada, 2020). This region is the largest population centre west of Southern Ontario and accounts for nearly 10% of Canada's Gross Domestic Product (GDP) in 2017 (Statistics Canada, 2020).

This region is also home to several Department of National Defence (DND) Facilities. There are two primary centres: Canadian Forces Base (CFB) Esquimalt and CFB Comox. CFB Esquimalt is home to the Maritime Forces Pacific and the Joint Task Force Pacific Headquarters. CFB Esquimalt consists of approximately 1,500 buildings over 12,000 acres of land and employs over 7,000 military and civilian personnel. CFB Comox is home to 19 Wing Comox and the Canadian Forces School of Search and Rescue. CFB Comox is the primary air operations installation on the Pacific Coast. It also operates Search and Rescue operations across B.C., the Yukon, and 1200 km out into the Pacific Ocean. Both facilities are expected to play important roles in supporting civil authorities following a significant, damaging earthquake.

4.2 SEISMIC HAZARD

In addition to being a centre for DND operations, SWBC is a region of high seismic activity and among the highest seismic hazard and risk in Canada (Onur, 2001 and Figure 1). Approximately 600 to 1,000 earthquakes occur in this region per year (Earthquakes Canada, 2021). The hazard in this region is a result of colliding tectonic plates. Offshore of Vancouver Island (and the Western United States as far south as Northern California), the oceanic Juan de Fuca plate subducts below the continental North American plate (Figure 2). This region, over 1,000 km long, is called the Cascadia Subduction Zone. The stresses between and within these plates result in three primary earthquake sources: large events on the subduction interface, shallow crustal events in the North American plate, and deep events within the subducting Juan de Fuca plate.

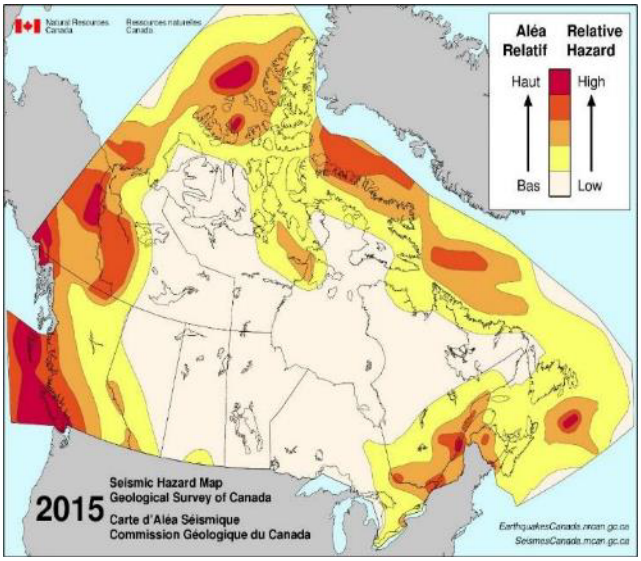

Figure 1: Simplified National Seismic Hazard Map produced from the 5th Generation seismic hazard model for Canada (Halchuk et al., 2015).

Along the Cascadia Subduction Zone interface, the Gorda, Juan de Fuca, and Explorer oceanic plates move eastward underneath the continental North American plate (Wang et al., 2003; Bostock et al., 2019). As the oceanic plates subduct, they interact with the overriding plate. The behaviour of this interaction changes with depth due to physical changes at the interface (Hyndman and Wang, 1993). At shallow depths, where the interface temperature is between 150°C and 350°C, the subducting plates are locked, meaning there is no relative motion between the subducting plate and the overriding continental plate (Hyndman and Wang, 1993; S. Li et al., 2018). Below the locked zone (between 350-450°C), the plates transition from fully locked to freely slipping past one another (solid line in Figure 2B).

In Cascadia, due to the warm subducting oceanic plate, the upper limit of the locked zone is believed to occur within 5km of the surface (Hyndman and Wang, 1993; Hyndman, 2013).

Meanwhile, the change from locked to transitional behaviour occurs around 12 km deep (Oleskevich et al., 1999; Hyndman, 2013; Schmalzle et al., 2014). Furthermore, the two plates begin to slide smoothly when the interface reaches approximately 25 km deep. The exact depths of these transitions vary along the strike of the interface as the 150°C, 350°C, and 450°C isotherms are not at constant depths and vary with differences in plate age, sediment thickness, and heat flow (Oleskevich et al., 1999).

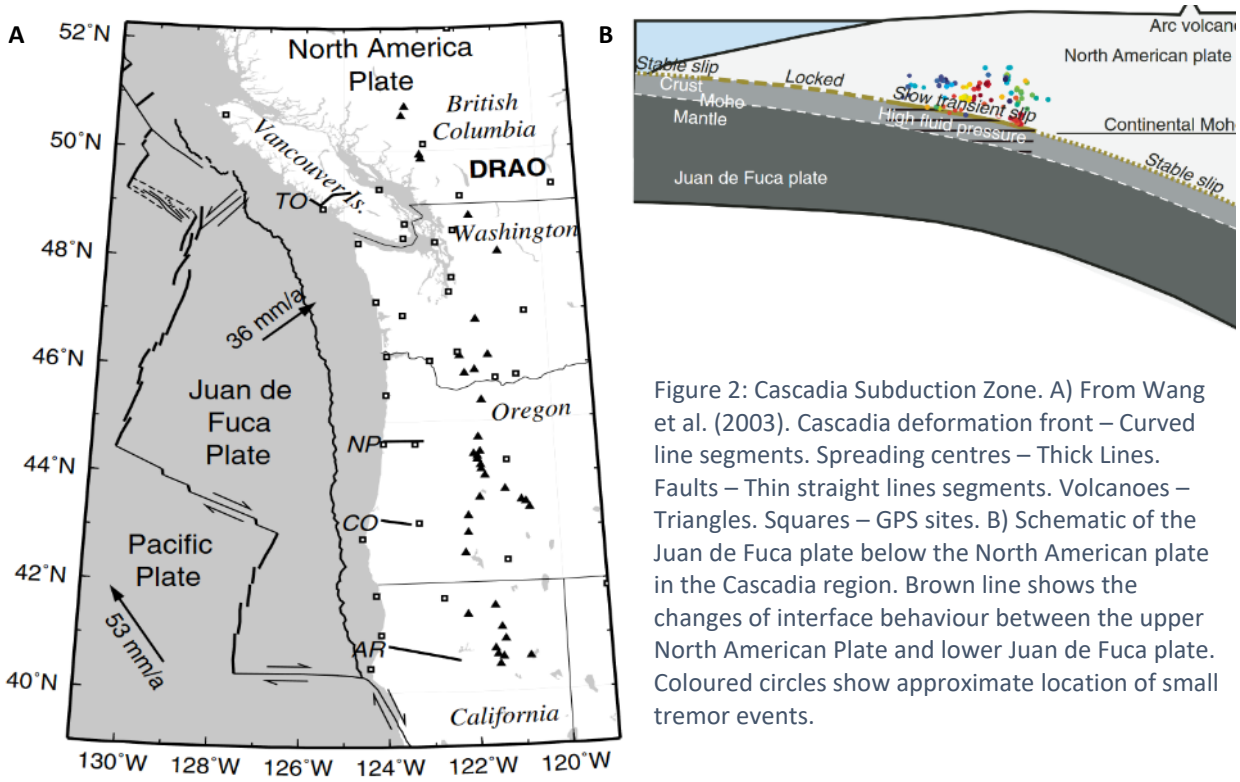

Figure 2: Cascadia Subduction Zone. A) From Wang et al. (2003). Cascadia deformation front – Curved line segments. Spreading centres – Thick Lines. Faults – Thin straight lines segments. Volcanoes – Triangles. Squares – GPS sites. B) Schematic of the Juan de Fuca plate below the North American plate in the Cascadia region. Brown line shows the changes of interface behaviour between the upper North American Plate and lower Juan de Fuca plate. Coloured circles show approximate location of small tremor events.

The Cascadia locked zone currently has little seismic activity, and therefore we observe few earthquakes on the interface. In the future, when the stress overcomes the locking friction, it will be released in a subduction (megathrust) earthquake. Megathrust earthquakes are the most significant earthquakes worldwide and can exceed magnitude 9. The large magnitude of these events means the shaking can be very intense, last for several minutes, and affect a broad area. Paleoseismic studies have determined that 19 to 23 of these events have occurred in the Holocene in Cascadia (Goldfinger et al., 2017) with a recurrence interval of 432 ± 160 years and a magnitude range of 8.85 ± 0.16 Mw (Kolaj et al., 2020). We can see that these events dominate the overall earthquake hazard in many parts of southwest BC, as shown in the seismic hazard deaggregation plots (Figure 3).

Once the oceanic plates move beyond the locked and transition zones, they begin to move smoothly beneath the overriding North American plate (Figure 2). As the depth of these plates increases, so do the temperature and pressure. This increase in temperature and pressure causes the oceanic plates to undergo chemical and physical changes.

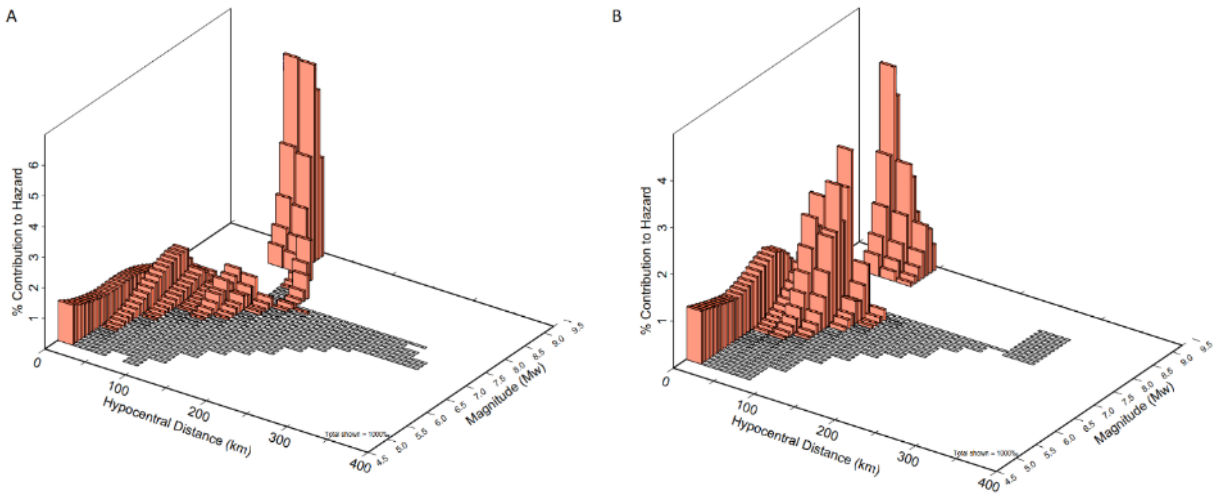

Figure 3: Seismic deaggregation plots for 2%/50 years hazard for two locations within SWBC; A – CFB Comox and B – CFB Esquimalt (Earthquakes Canada, 2020). Largest contributor in both cases (M>8.5 and distances > 50 km) is the Cascadia Megathrust. The second most hazardous source type for CFB Comox is nearby (< 50 km), more moderately sized (M < 8) crustal events. Meanwhile CFB Esquimalt has additional hazard from close crustal events and more distal larger events, such as in-slab 2001 Nisqually style events.

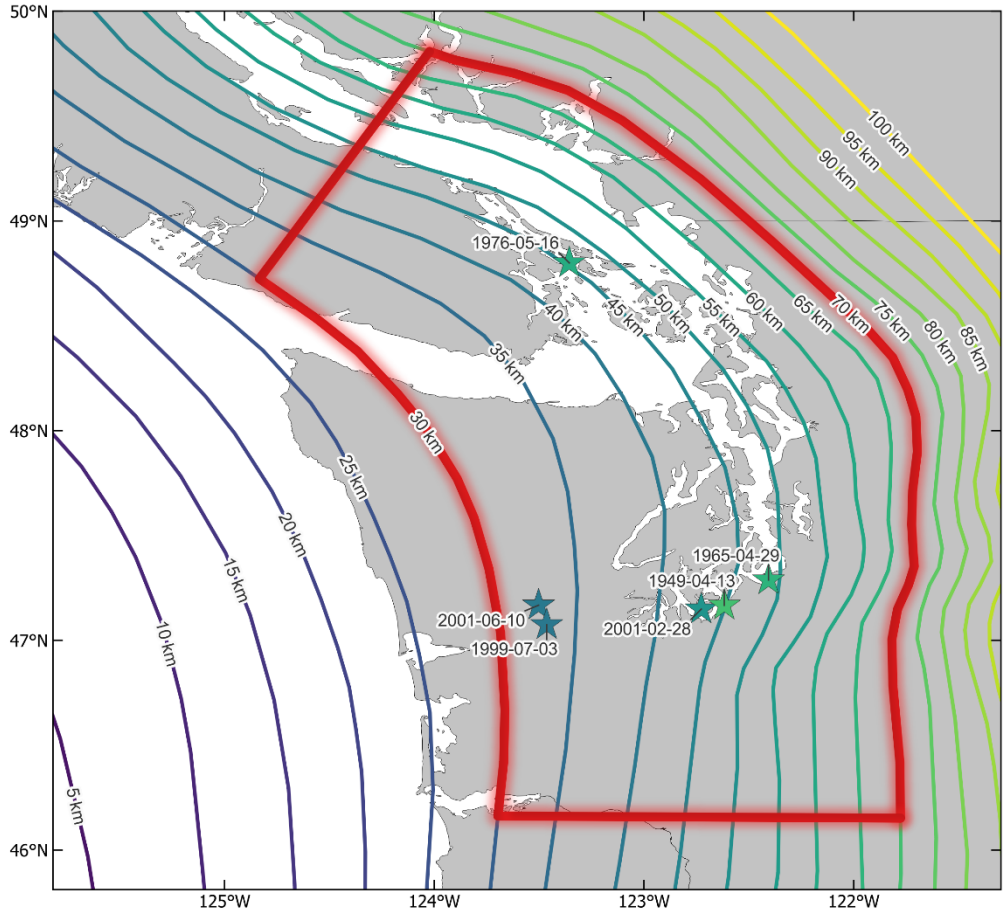

Figure 4: Location of in-slab earthquakes M>5 in Cascadia with depths shown following depth contour colouring. Red outline is the area where in-slab earthquakes are likely. Depth contours of the subducting Juan de Fuca slab from McCrory et al. (2012).

Table 1: Significant in-slab earthquakes in the Cascadia region. Intensity is the maximum shaking intensity felt for each event as reported by the USGS (2020).

Date	**Latitude (°N)**	**Longitude (°W)**	**Depth (km)**	**Magnitude (M_w)**	**Intensity**
2001-06-10	47.17	123.50	40.2	5.0	V
2001-02-28	47.15	122.73	51.8	6.8	VII
1999-07-03	47.07	123.46	40.0	5.8	V
1976-05-16	48.8	123.4	62	5.1	IV
1965-04-29	47.4	122.3	59	6.7	VII
1949-04-13	47.17	122.62	70	6.8	VIII

Dehydration and other phase change reactions, such as basalt-to-eclogite transformation, make the slabs brittle (Kirby, 1995; Peacock and Wang, 1999). In northern Cascadia, at least ten significant in-slab ruptures have occurred in modern times, with six being instrumentally observed (Figure 4 and Table 1) (Saragoni and Concha, 2004). The three largest earthquakes (1949, 1965 and 2001) resulted in widespread damage, at least one death, and many injuries (Preston et al., 2003). For example, the 2001 Nisqually event caused injuries to four hundred people and created an estimated 1 to 4 billion USD in damage (Highland, 2003).

When we combine the plate bending and chemical changes to the slab occurring at 40-70 km depth (Kao et al., 2008) with plate geometry (McCrory et al., 2012) and the extent of subduction (Audet et al., 2009), we can determine the in-slab source region (Figure 4). This zone lies directly below some of this region's most populated areas.

The third primary hazard source, crustal earthquakes, occur in the overriding North American plate (Figure 5). The stress that causes these earthquakes comes from the nearby subduction zone, where locking between the two plates causes the deformation of the overriding North American plate.

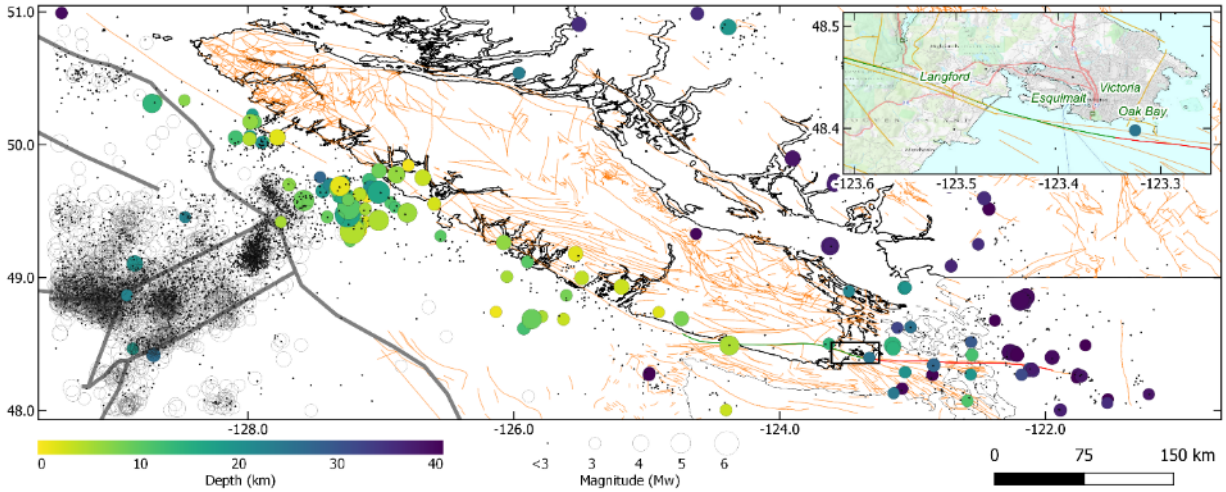

Figure 5: Crustal Seismicity of Southwestern British Columbia 1980-2020 (Earthquakes Canada, 2020). Dots are earthquakes M_w<3. Open circle are earthquakes with manual set depth (10 km), while closed circles are coloured by depth. Orange lines are mapped geological faults, some faults are only mapped to the USA-Canada border but are likely to continue. Grey thick lines are tectonic boundaries. Green line is the Leech River Valley Fault and red is the Devil's Mountain Fault. Inset shows the location where the two faults meet south of Victoria/Oak Bay.

These earthquakes are often much lower in magnitude, but in rare, low-occurrence cases, can be significant events. For example, the M_w 7.3 1946 Vancouver Island earthquake (Hodgson, 1946; Rogers and Hasegawa, 1978). Some crustal sources are well-known active faults (such as the offshore Nootka

Fault Zone) with significant amounts of observed seismicity (Merrill et al., 2022). A second group with fewer or no observed earthquakes but other geophysical evidence of past ruptures exists (i.e., Leech River Valley-Devil's Mountain Fault, Whidbey Island fault zone, Beaufort Range Fault). A primary example of this type of fault is the Leech River Valley-Devil's Mountain Fault (LRV-DMF). The LRV-DMF is located across Southern Vancouver Island and extends eastward into northwest Washington State (Figure 6), and consists of two characterized sections: the Devil's Mountain Fault and the Leech River Valley Fault. Johnson et al. (2001) characterized the Devil's Mountain portion and determined that the DMF originates in western Washington at Devil's Mountain south of Whitney and extends westward for 125 km across the Salish Sea to just south of Oak Bay, BC. They also show that the DMF is N/NE dipping between 45 and 75° in the upper 2 km with a left-lateral oblique motion. Barrie and Greene (2018) and Barrie et al. (2021) determined that the DMF extends to meet the Leech River Valley Fault (LRVF) south of Greater Victoria. The LRVF trace continues from south of Victoria northwest up the Leech River Valley and across Vancouver Island (Figure 5). The fault continues offshore at Sombrio point, crossing the Juan de Fuca strait, terminating at the Tofino Fault. The LRVF extends to similar depths as the DMF and is dipping steeply to the northeast (Li et al., 2018). Recent studies have shown Holocene (<10 000 years) activity along the LRVF (Harrichhausen et al., 2021). Morell et al. (2017) determined that multiple M > 6 earthquakes have occurred in the last 15 ka. Fault length to magnitude relationship suggests that the LRV-DMF has the capacity to produce M7-7.5 earthquakes (Wells and Coppersmith, 1994; Stirling et al., 2013).

5 METHOD

5.1 REGION AND TARGETS OF INTEREST

The primary goal of this analysis is to model the scenario hazard for key DND assets in SWBC. To conduct this analysis, we needed to collect the location of the assets of interest. Since DND personnel live both on and off base, and DND is expected to be able to actively support civil authorities after a large earthquake, we should also consider the hazard to the communities surrounding the DND bases.

5.2 SOFTWARE

NRCan uses Global Earthquake Model's OpenQuake software (GEM Foundation, 2020; Pagani et al., 2014) to conduct scenario hazard modelling (Hobbs et al., 2021). OpenQuake has several required inputs for its calculations. For a hazard calculation, the first input needed is the locations of the sites of interest. Next is the site condition model, representing how local geological conditions modify seismic waves. The third input is the ground motion model (GMM). These models describe how the seismic energy travels through the earth from the earthquake source to the measurement sites. GMMs are commonly empirical functions of distance, earthquake source type, regional and local site conditions. The last input is the earthquake source: the information on the earthquake location, magnitude, rupture area, and rupture motion (earthquake type).

5.3 SITES OF INTEREST

As discussed above, we are interested in the hazards on DND properties and within the surrounding communities (Figure 6). To ensure that we covered the region sufficiently, we combined three location datasets. The first is the location of assets owned or of interest to DND. Andrew MacDonald (personal communication, 2020) collected, compiled, and provided these locations. Similarly, Journeay et al. (2022) provided previously compiled locations of general population assets for

the surrounding communities. In addition to the provided sites above, we know the hazard extend beyond populated areas. Outside of towns/cities, additional infrastructure (e.g., dams, pipelines, power connections, roadways) may be of interest in the future but are not in the previous two datasets. Therefore, we included sampling locations outside the populated areas using a 1 km x 1 km grid. Combining of these three datasets provides ample coverage of the study region (Figure 7).

5.4 Site Conditions

Site conditions are typically measured using V_{S30}, the average shear-wave velocity in the upper 30m of the earth. V_{S30} can be measured through seismic methods, boreholes, or estimated by local geology and slope (Allen and Wald, 2007; Motazedian et al., 2011). We collected V_{S30} values used in this study from four sources and combined them into a single dataset. The first dataset is V_{s30} values measured directly using spectrum analysis of surface waves (Hunter et al., 1998). The second data set includes estimates from surface geology and borehole data (Greater Victoria - Monahan et al., 2000; Lower Mainland - Taylor et al., 2006). Outside of these population centres, we needed to estimate the V_{S30} as no direct or inferred values existed. We used the approximation of V_{S30} from the topographic slope by Allen and Wald (2007). We sampled all these datasets at the sites of interest (Figure 7 and electronic supplement).

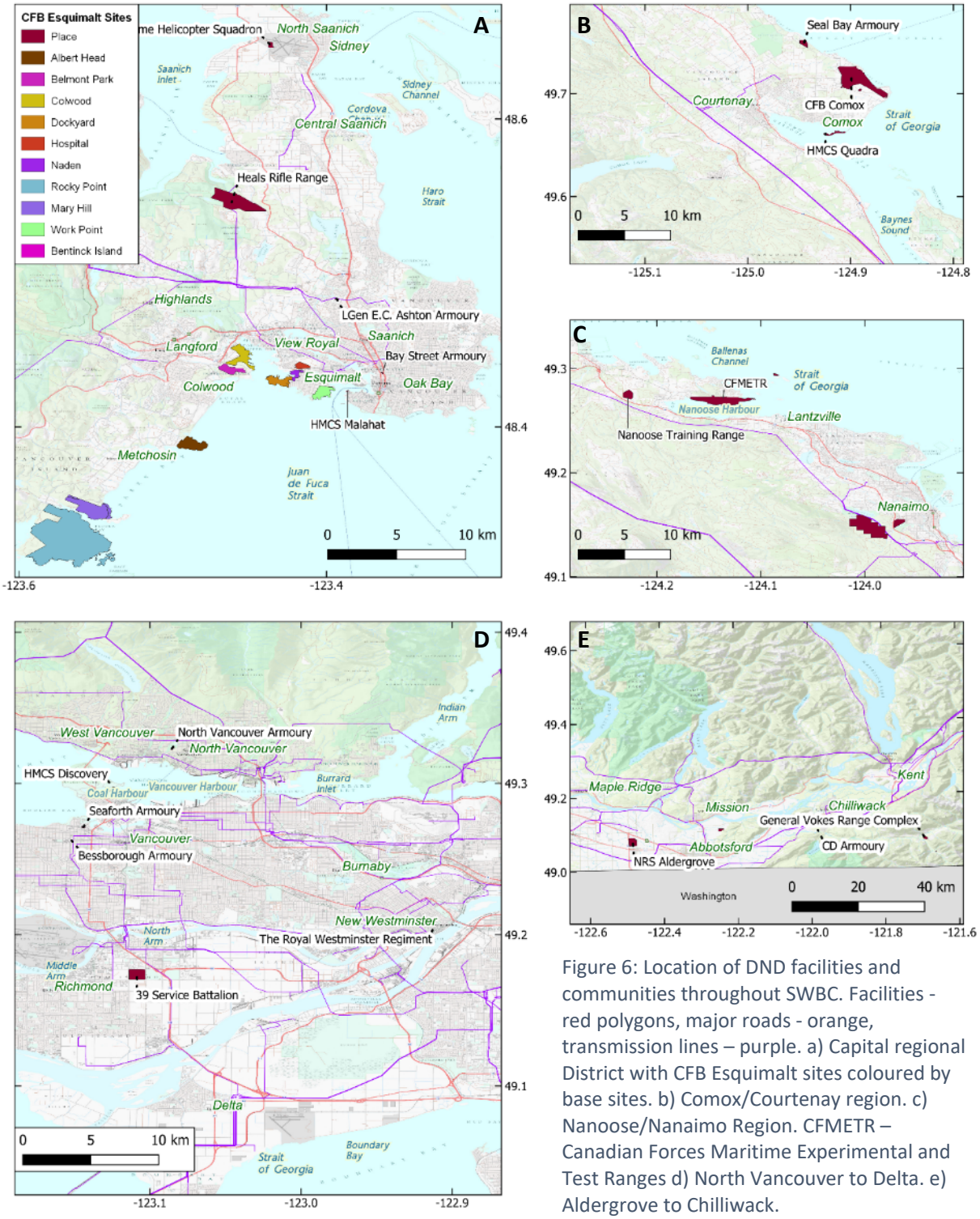

Figure 6: Location of DND facilities and communities throughout SWBC. Facilities - red polygons, major roads - orange, transmission lines – purple. a) Capital regional District with CFB Esquimalt sites coloured by base sites. b) Comox/Courtenay region. c) Nanoose/Nanaimo Region. CFMETR – Canadian Forces Maritime Experimental and Test Ranges d) North Vancouver to Delta. e) Aldergrove to Chilliwack.

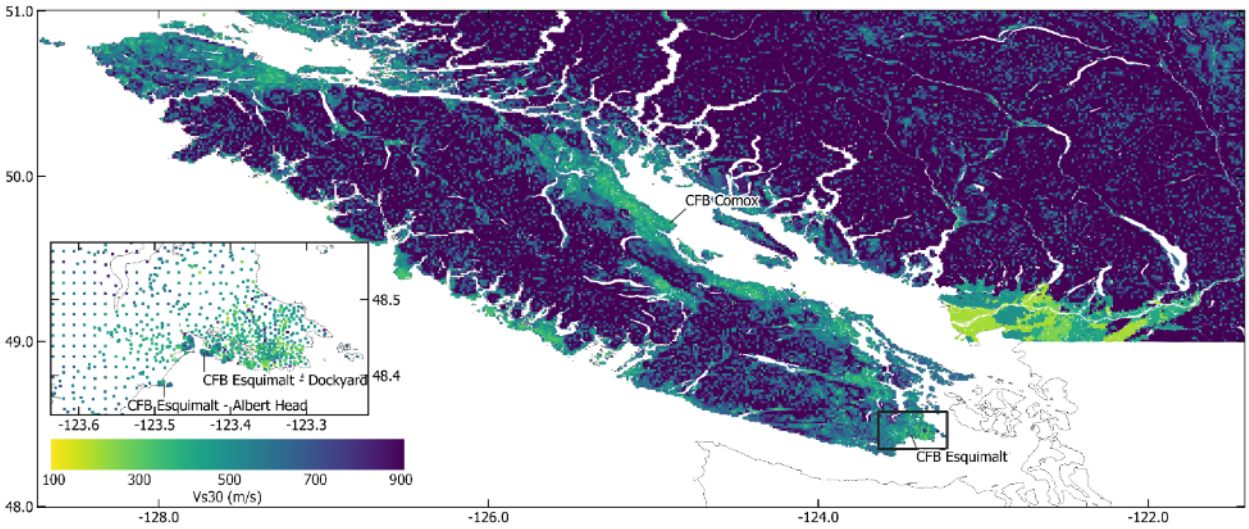

Figure 7: V_{S30} values of Southwestern British Columbia and Greater Victoria.

Table 2: Ground Motion Model sets used in the scenarios. Each scenario used a different set of weighted GMMs based on the earthquake type. In some cases, GMMs have been modified by Kolaj et al., (2020) from their original references to be more appropriate in Canada.

Scenario	Ground Motion Model	Weight	Reference
Subduction	AbrahamsonEtAl2015Sinter	0.25	Modified from Abrahamson et al. 2015
	AtkinsonMacias2009NBCC2020	0.25	Modified from Atkinson and Macias 2009
	GhofraniAtkinson2014CascadiaNBCC2020	0.25	Modified from Ghofrani and Atkinson 2014
	ZhaoEtAl2006SInterCascadiaNBCC2020	0.25	Modified from Zhao et al 2006
In-slab	AbrahamsonEtAl2015SSlab	0.25	Abrahamson et al 2015
	AtkinsonBoore2003SSlabCascadiaNBCC2020	0.25	Modified from Atkinson and Boore 2003
	GarciaEtAl2005SSlabNBCC2020	0.25	Modified from Garcia et al 2005
	ZhaoEtAl2006SSlabCascadiaNBCC2020	0.25	Modified from Zhao et al. 2006
Crustal	AbrahamsonEtAl2014	0.25	Abrahamson et al 2014
	BooreEtAl2014	0.25	Boore et al. 2014
	CampbellBozorgnia2014	0.25	Campbell and Bozorgnia 2014
	ChiouYoungs2014	0.25	Chiou and Youngs 2014

5.5 Ground Motion Models

We selected the ground-motion models (GMMs) from those used by Canada's Generation Six Seismic Hazard Model (CanSHM6) (Kolaj et al., 2020). In CanSHM6 and our scenarios, instead of using a single GMM per earthquake, four different GMMs with equal weighting (Table 2) are employed, to encompass the epistemic uncertainty.

5.6 Selection of Earthquake Scenarios

Given the three distinct types of earthquakes in the Cascadia subduction zone, we have selected a scenario for each type – subduction, in-slab, and crustal. For the Cascadia subduction zone, using the information compiled by Goldfinger et al. (2017) and Kolaj et al. (2020), as discussed above, we determined that our event must fit in the expected moment magnitude of 8.85 ± 0.16. We created a Cascadia Megathrust scenario with a hypocentre at 48.83 °N, -126.92°W at a depth of 5 km and a moment magnitude of 8.9 (Figure 8a). This location coincided with the largest rupture patch observed in models of the most recent Cascadia earthquake (Wang et al., 2013). We considered the earthquake to rupture the entire locked zone and extend into the transition zone for our subduction model. The extension into the transition zone is to accommodate the findings by Hyndman (2013) that determined any Cascadia earthquake rupture should include 50% of maximum slip to occur within this transition zone. Due to constraints in the modelling software (unable to produce partial slip), we approximated this 50% slip by allowing full rupture across half of the transition zone. We used 4, 12, and 18 km depths for the up-dip, locked zone, and half transition zone depth limits. We selected these depths from the thermal limits of Hyndman and Wang (1993) and Hyndman (2013) (as discussed in section 4.2) and the 1D temperature models of Oleskevich et al. (1999). We determined the location of these depths using the interface surface of McCrory et al. (2012). We consider the extension into the transition zone to be a moderate case as it does not consider the transition zone fully locked, producing the most damaging style event inland. However, it does not consider the locked zone the only energy source – potentially the least damaging event.

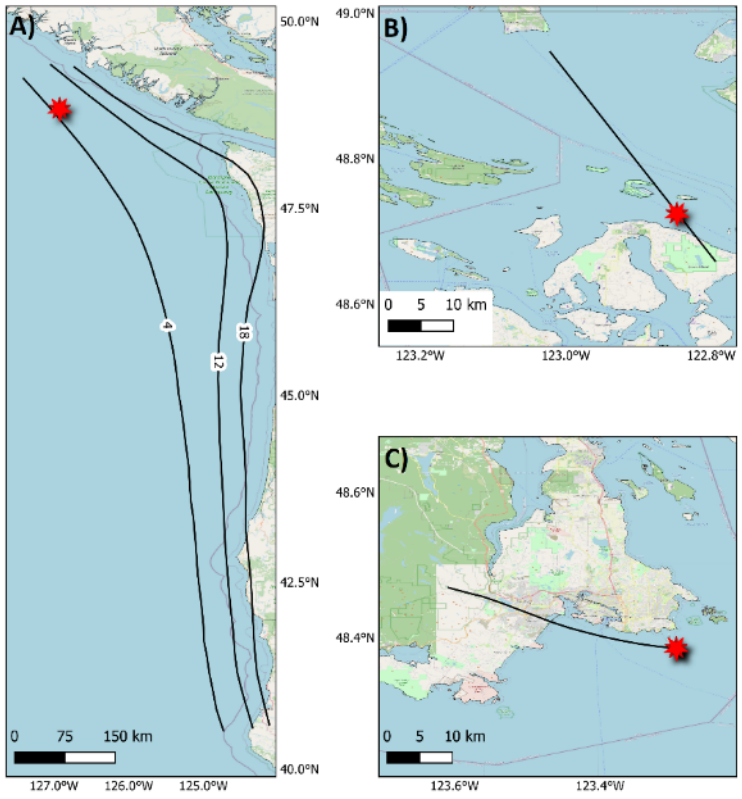

Figure 8: Three earthquake scenarios. Red star - epicentres A) Cascadia Subduction zone with depth contours of rupture surface. B) In-slab scenario with upper trace of fault plane in black. C) Crustal scenario with upper trace of fault plane in black.

For the In-slab earthquake scenario, we placed our scenario at 48.72°N, -122.85°W with a depth of 57 km (Figure 8b). We set the rupture to occur asymmetrically along a plane between 48.66°N, -122.79°W and 48.95°N, -123.02°W between 50 to 60 km depth. We set the earthquake magnitude to 6.8 to be like the 2001 Nisqually event.

Determining a representative crustal event scenario is more challenging than the last two scenario types. Crustal events in this region have a large spatial variability (Figure 5) and the frequency of occurrence of a specific crustal event in this region is unknown. Due to the wide variability of possible crustal events (Figure 5), we considered several earthquakes throughout the region. Bearing in mind the target of the hazard analysis is to construct valid but still challenging scenarios, we selected a moderate to large earthquake along the Leech River Valley-Devil's Mountain Fault (LRV-DMF) to represent a crustal source. Specifically, we selected to model an M6.4 earthquake rupturing along the LRV-DMF initiating at 48.38°N, -123.22°W and 5 km depth (Figure 8c). We also chose the seismogenic zone with depths between 1 and 15 km with a dip matching the dip observed for the DMF by Johnson et al. (2001).

5.7 PROCESSING

We used the ground conditions, ground motion models, and the three rupture scenarios we described above in OpenQuake and standard input parameters for scenario hazard analysis (GEM, 2020). We ran each scenario one thousand times, 250 times per GMM; this was done to capture the aleatory variability of the rupture processes. The GMMs contain information about epistemic uncertainty, and we only allowed results to fall within three standard deviations of the mean GMM. We retrieved the resulting ground motion fields (GMFs) and processed them using python scripts to determine the 0.25, 0.50 (median), and 0.75 quantiles. We included a sample input 'ini' file and the complete data set in the electronic supplement.

6 PRIMARY HAZARD RESULTS

6.1 M8.9 SUBDUCTION

We present the first scenario with the Mw 8.9 subduction style event along the Cascadia interface (Figure 8a). The median Peak Ground Accelerations (PGA) (Figure 9) shows one measure of the shaking that the Cascadia Megathrust earthquake scenario produces in SWBC. As expected, the shaking levels experienced are the greatest nearest to the rupture plane with a max PGA of 0.44g (44% of average acceleration due to gravity) experienced on the west coast of Vancouver Island (~50 km NW of Tofino, BC. The PGA, in general, decreases towards the northeast, away from the subduction zone. We see exceptions to the trend along the east coast of Vancouver Island and the Fraser River/Delta. These areas experience amplification due to the decrease in V_{S30} from these more sediment-laden areas (Figure 7). We can estimate the perceived shaking using Worden et al.'s (2010) relation between PGA and Modified Mercalli Intensity (see legend in Figure 7). Using this relation, we can see that the experienced shaking will be heavy to violent on the west coast of Vancouver Island, reducing to light in the Coast Mountains or further up the Fraser Valley, but felt across the entire study region. In addition to the PGA, we calculated eight additional ground motion fields. These additional fields were Spectral accelerations (SA) at periods of 0.1, 0.2, 0.3, 0.5, 0.6, 1.0, 2.0, and 5.0 seconds.

CFB Comox will experience modest shaking, meanwhile CFB Esquimalt will experience up to very strong shaking (CFB Esquimalt – Rocky Point) (Figure 10). Meanwhile, smaller facilities throughout Greater Vancouver experience modest shaking. The variation in ground shaking across a single facility is minimal at CFB Comox, Nanoose and Nanaimo facilities. These small changes in hazard are due to the

small size of the bases relative to the distance to the rupture plane. Meanwhile, CFB Esquimalt has several visible changes across the base sites. Particularly, Rocky Point has a PGA up to 20% of gravity (g) at the centre of the base, down to values of 16% of g near the shore. We observe similar relative changes (~80% reduction) at all measured spectral accelerations for these sites. This change in hazard is primarily due to the increase in V_{S30} between the centre of the Rocky Point, which is bedrock blanketed by glacial till (>1 m in thickness) and the shoreline formed of bedrock and weathered bedrock veneer (Blyth and Rutter, 1993).

We can also analyze the hazard of DND facilities through hazard spectra, which is a plot of the intensity of shaking versus the period of spectral acceleration (Figure 11). We determined from the spectra that the energy released from the scenario event is dominated near 0.5 s period. The direct hazard to specific buildings in this region is dependent on the construction method and natural period of each building. In general, however, it can be approximated that the most affected building height, in storeys, will be ten times the dominant period. Thus, with SA being largest at 0.5 s period, or 2Hz frequency, it implies that multi-storey buildings will have the strongest response to this earthquake.

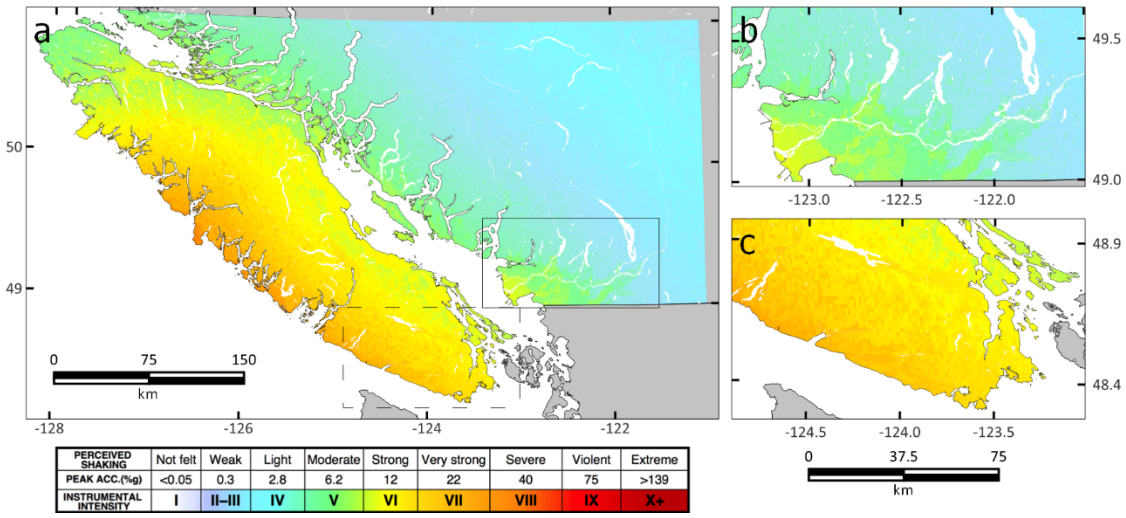

Figure 9: Peak Ground Acceleration due to the Cascadia Megathrust scenario. PGA to perceived shaking is modified from Worden et al. (2010).

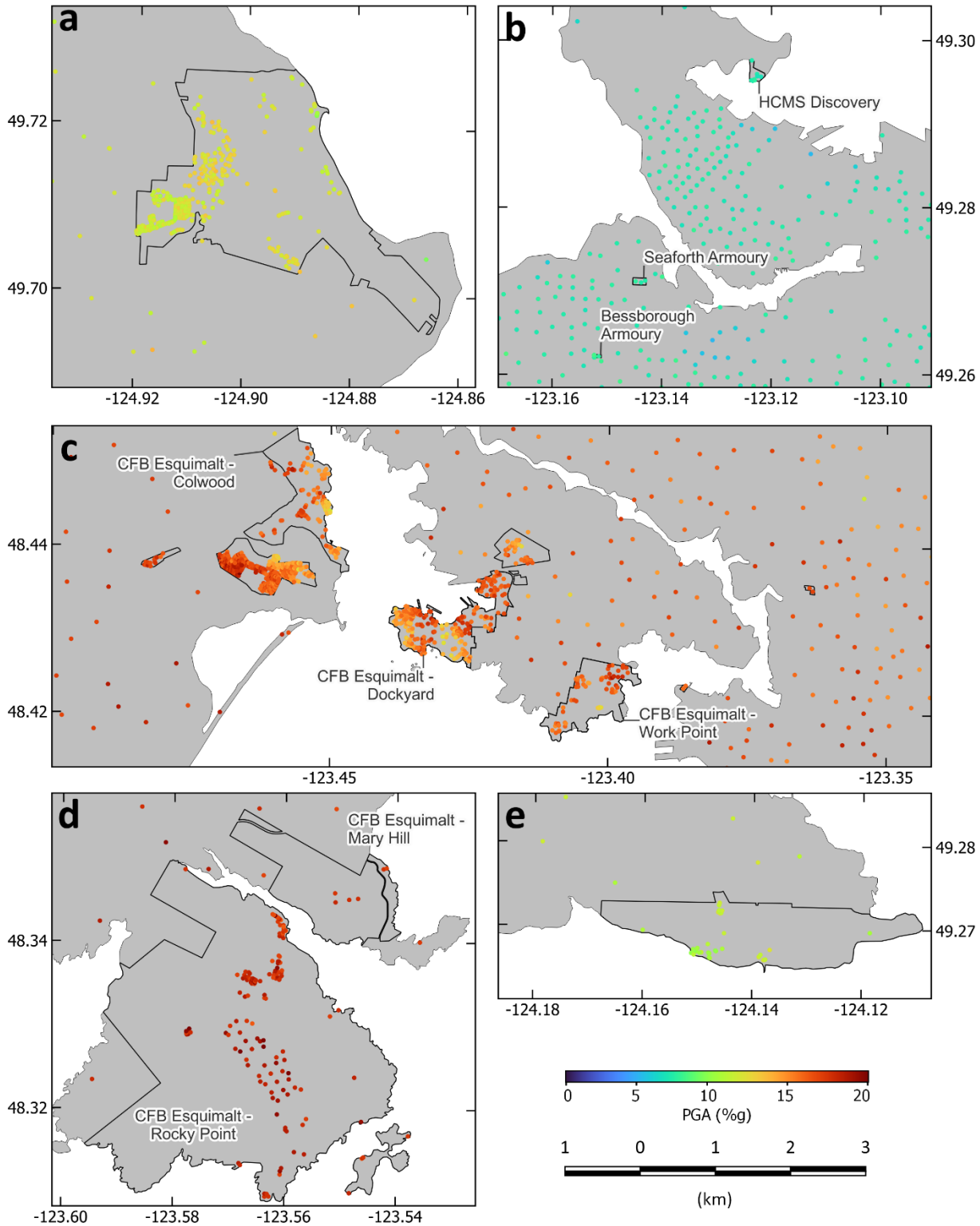

Figure 10: PGA of select DND sites. Outlines of DND bases are shown with black lines. Sample points are irregular due to the distribution of DND and general population assets (see section 5.4). a) CFB Comox b) Vancouver c) CFB Esquimalt Dockyard, Work Point, and Colwood sites d) CFB Esquimalt Rocky Point and Mary Hill e) CFMETR at Nanoose Bay.

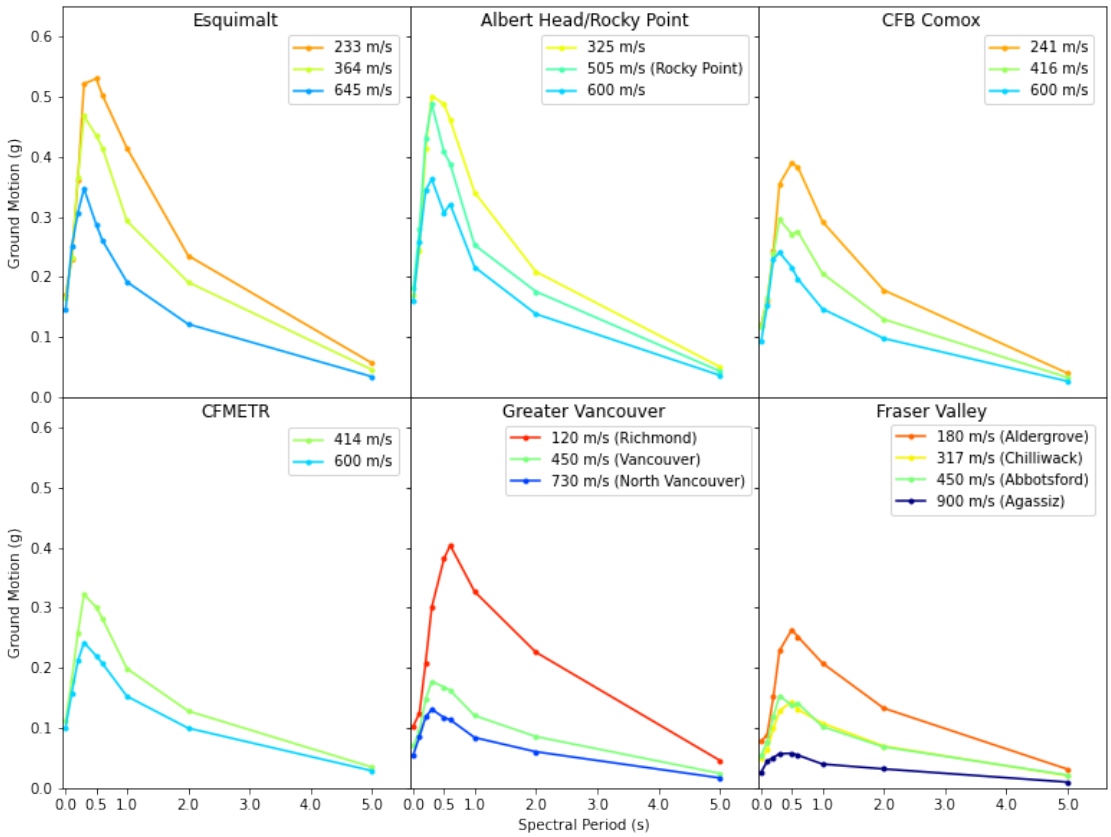

Figure 11: Hazard Spectra of DND asset locations in the Cascadia Scenario. Spectral period of 0 s is the PGA component. Legend values are V_{S30} of the sample locations. The distribution of ground motion is similar across the region with the changes to the shape due to the differences in attenuation at greater distances.

6.2 In-slab

The M6.8 In-slab event with a rupture plane 50 km below Boundary Bay has a much-reduced affected region than the Cascadia event due to this earthquake being 2.1 magnitude units smaller (~1400 times less energetic). Though smaller, this earthquake still creates significant shaking in areas close to the hypocentre, such as the lower mainland (Figure 12). The shaking intensity reduces with distance from the epicentre, except for significant amplification in the sediments of the Fraser River. Victoria and CFB Esquimalt experience more modest shaking relative to the Cascadia scenario. Meanwhile, CFB Comox, being an additional 175 km away, experiences felt but light shaking (Worden et al., 2010).

Seven SA at differing periods (0.1, 0.2, 0.3, 0.5, 0.6, 1.0, and 2.0 seconds) were also calculated. We did not calculate SA(5.0) due to limitations in the GMMs used for this scenario. We consider this to be acceptable as we found that the SA is largest between 0.1 to 0.5 second periods and strongly decays in intensity towards SA(2.0) (Figure 13). The hazard spectra across the region shows Greater Vancouver experiencing greater SA values than for the Cascadia subduction scenario. For this in-slab scenario, we determined that the 0.3 seconds SA dominates at both CFB Esquimalt and CFB Comox.

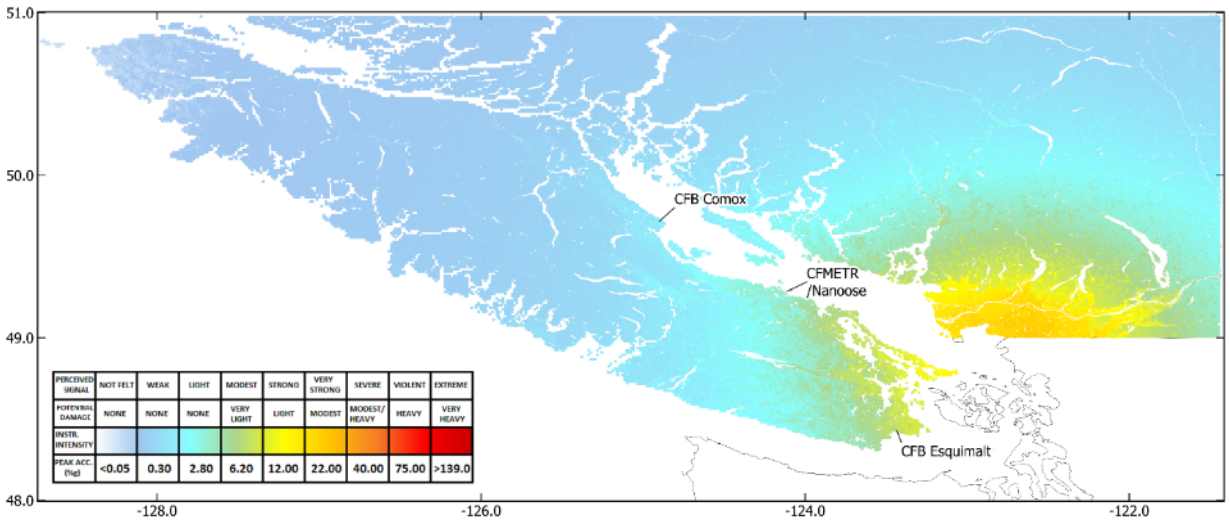

Figure 12: Peak Ground Acceleration due to the in-slab scenario. The event is localized to Greater Vancouver with additional strong shaking across to Southern Vancouver Island. PGA to perceived shaking is modified from Worden et al. (2010).

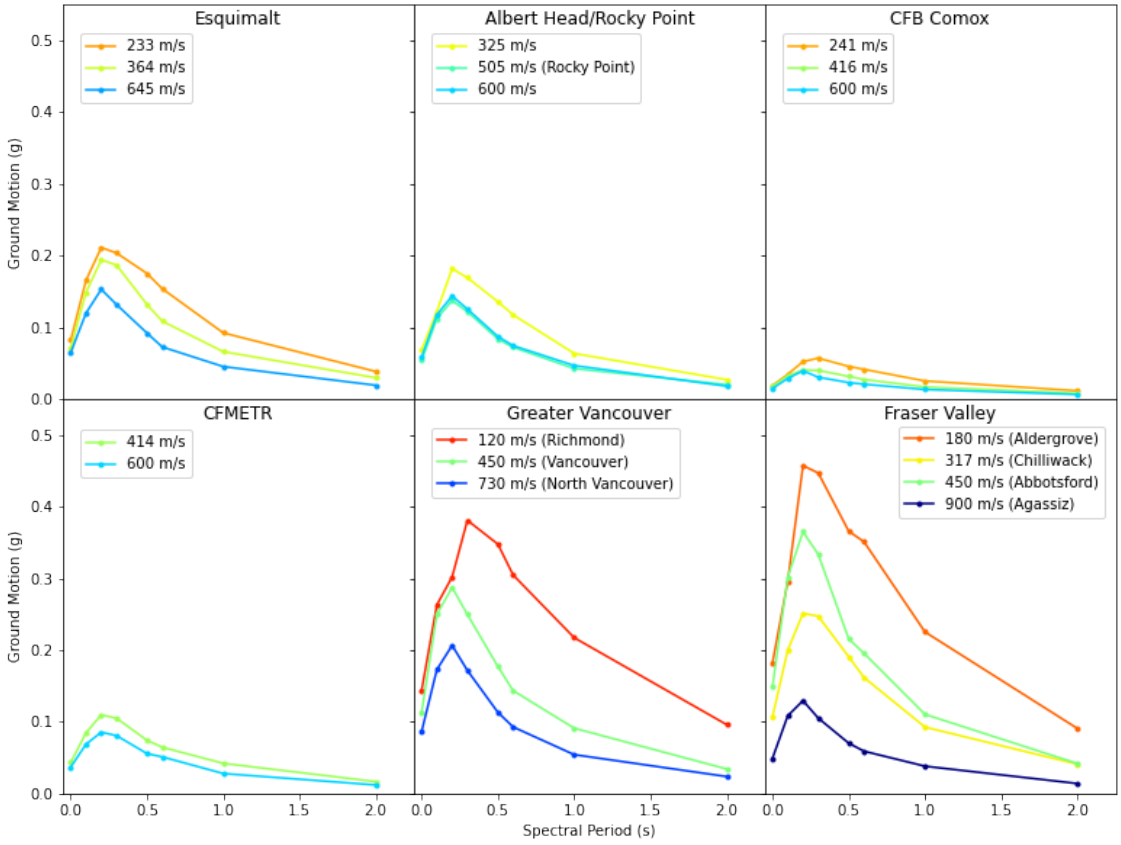

Figure 13: Hazard Spectra of DND asset locations in the in-slab scenario. Spectral period of 0 s is the PGA component. Legend values are V_{S30} of the sample locations. The distribution of ground motion varies across the region with high amplitude broad spectra throughout Greater Vancouver, meanwhile other locals within the region see lower amplitude ground motion.

6.3 CRUSTAL

The Leech River Valley – Devil's Mountain Fault scenario was the smallest magnitude of our three scenarios at M_w 6.4. This scenario occurs along a shallow rupture plane (1 to 30 km deep) following the LRV-DMF trace offshore of Greater Victoria towards the Leech River Valley. The PGA map (Figure 14) shows that although it is the smallest magnitude event, the proximity to greater Victoria yields the highest amplitude of shaking (maximum PGA of 0.58g experienced in Langford). The ground-shaking drops off to modest shaking at ~75 km from the rupture plane and light shaking within 150 km. The quick attenuation of the shaking intensities means that only light shaking is experienced in most of Greater Vancouver and central Vancouver Island (including Comox). The amplification due to the soft soils of the Fraser River Delta generates modest shaking in Richmond.

Like the other two scenarios, we calculated the SA at differing periods (0.1, 0.2, 0.3, 0.5, 0.6, 1.0, 2.0, 5.0 and 10.0 seconds). Additionally, we calculated the Peak Ground Velocity (PGV). The hazard spectra display the extreme localization of shaking (Figure 15), as the peak amplitude in Victoria is five times that felt in Vancouver on similar soil and more than ten times that in Nanaimo.

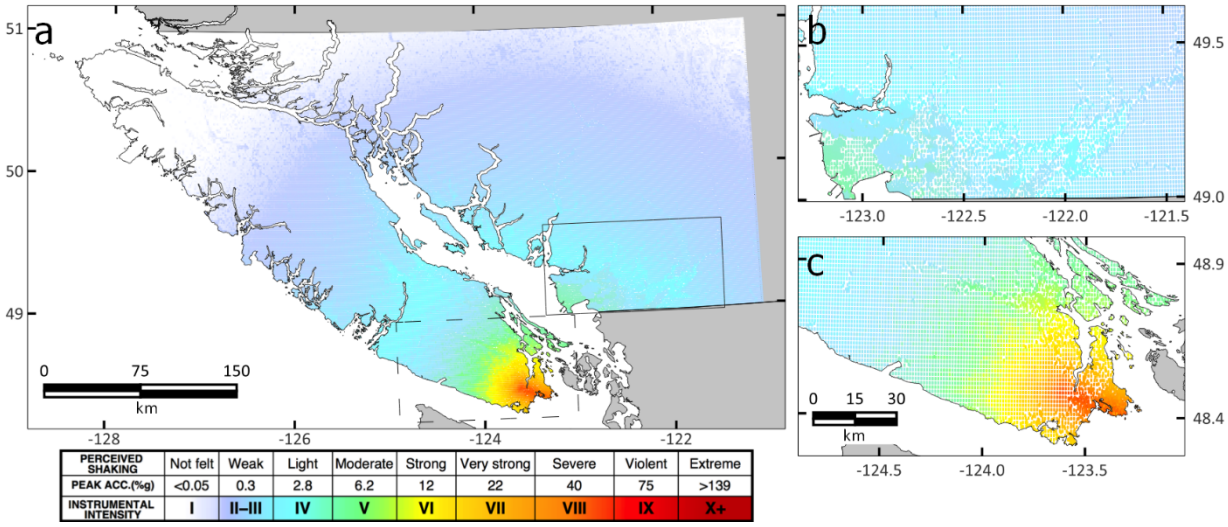

Figure 14: Peak Ground Acceleration of the Leech River Valley-Devil's Mountain Fault scenario earthquake. Highly localized extreme shaking. PGA to perceived shaking is modified from Worden et al. (2010).

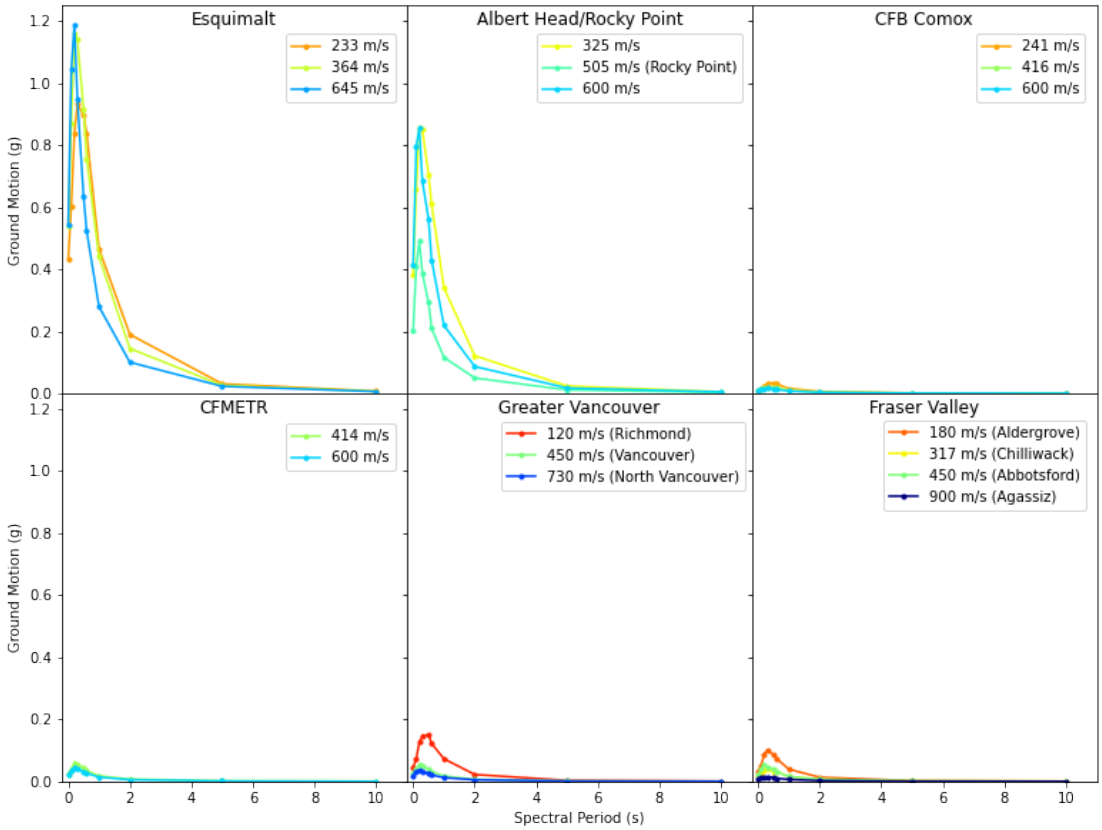

Figure 15: Hazard Spectra of DND asset locations in the crustal scenario. Spectral period of 0 s is the PGA component. Legend values are V_{S30} of the sample locations. Significant (>50% of g) is experienced in Esquimalt for PGA to spectral periods of 0.5 seconds. This shaking is still substantial at Albert Head but has a steep drop off at further distances.

7 SECONDARY HAZARDS

In addition to the primary shaking, there are additional secondary hazards related to earthquakes that can have significant effects:

1. Surface rupture and tsunami, resulting directly result from earthquake slip,
2. Secondary amplification factors, liquefaction, landslides, flooding, and fire (all of which are related to shaking),
3. Aftershocks - these are subsequent earthquakes (smaller than the mainshock) that occur due to changes in the stress field near an earthquake.

These secondary factors depend on the earthquake properties and the local geology.

7.1 Secondary Amplification Factors

In addition to the surface conditions (V_{S30}), basin and topographic effects can modify ground shaking and the resulting seismic hazard. Basin effects arise from a concave basement of bedrock overlain with soft sediments. Basin effects modify seismic hazard through two main processes. First, the basin can trap the seismic waves in the body of the basin. Secondly, the impedance contrast at the basin walls can focus the seismic energy. These two effects can significantly affect the ground motion's amplitude, duration, and frequency.

Past studies have observed the basin amplification due to the Georgia basin (Figure 16) and that this amplification extends into Vancouver (Kakoty et al., 2021). Due to modelling limitations, we have not explicitly determined the impact of any basin effects in our scenarios but expect that the addition of basin effects into the model would increase the shaking at some sites.

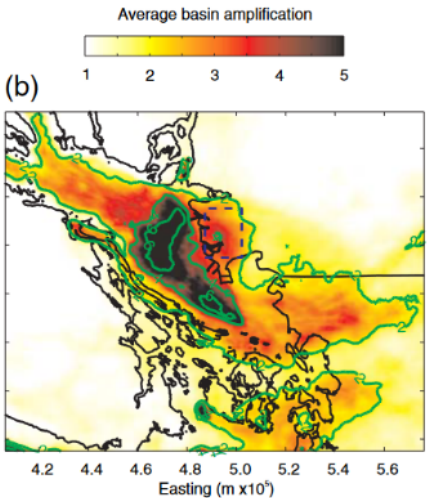

Figure 16: Basin Amplification due to the Georgia Basin. From Molnar et al. (2014).

Topographic amplification results from the "funnelling" of seismic energy towards the ridge or peaks of topographic features, creating amplification at these locations. Therefore, a site along a ridge or peak will have more vigorous shaking than a similar site in a valley bottom or flat region with the same site conditions. Due to modelling limitations, we omitted direct calculation of topographic amplification. Even without direct calculations we expect minimal impact as most DND sites have low topographic variations or are in valleys resulting in minimal topographic amplification. For example, CFB Comox has less than 20 m of elevation variation across the entire property.

7.2 Liquefaction

Liquefaction is when the ground becomes temporarily liquified when subjected to shaking from an earthquake. The probability and spatial distribution of liquefaction depend on the geological, groundwater, and seismic conditions (Youd et al., 2001; Jefferies and Been, 2015). Liquefaction is most probable in soft soils where the groundwater level is near the surface. Liquefaction can be a significant hazard during an earthquake, as seen in San Francisco's Marina District during the 1989 Loma Prima earthquake (Holzer, 1992), the 1964 Niigata Earthquake (Kawasumi, 1968), and more recently the 2011 Christchurch Earthquake (Cubrinovski et al., 2014). Curbinovski found that 97% of all major and 80% of moderate road damage occurred within regions of moderate or severe liquefaction during the 2011 Christchurch earthquake.

Several studies have mapped the liquefaction hazard in select municipalities in southwest British Columbia: Victoria - Monahan et al. (2000), Richmond – Monahan et al. (2010), Greater Vancouver – Taylor et al. (2006), and North Vancouver – Wagner et al. (2015). Due to the complex nature of the calculations for liquefaction, we have only considered the liquefaction hazard near major DND bases (CFB Comox and CFB Esquimalt) in our region; for other sites, we suggest reviewing the studies listed above. There are three primary measures of the liquefaction hazard that we reviewed. The first is the susceptibility, which is agnostic of the seismic hazard and is dependent on the ground conditions. Meanwhile, the liquefaction probability and the permanent ground deformation (PGD) are obtained directly from the scenario earthquake model.

We obtained surficial mapping across the region from several sources to determine the liquefaction hazard. For CFB Comox and area, we used the map of Fyles (1960). For CFB Esquimalt we combined the geology of Monahan et al. (2000) and Blyth and Rutter (1993). Additionally, we collected the approximate age information for the units (when not specified) from Clague and Ward (2011). We estimated the Liquefaction Susceptibility, Probability of Liquefaction, and ground deformation of each mapped unit using the process described in HAZUS (FEMA, 2020).

We found that liquefaction susceptibility is relatively low for these locations, with the notable exception of regions with significant anthropogenic fill or on river sediments (Figure 17). CFB Esquimalt at Rocky Point, William Head, Albert Head, Work Point, and Belmont Park have low to very low liquefaction susceptibility due to the near-surface bedrock and relatively minimal surficial sediments. CFB Esquimalt at the Dockyard and Colwood have low liquefaction susceptibility, except near shore where artificial fill dominates – notably, this is where most of the dock infrastructure resides. CFB Comox has moderate to high liquefaction susceptibility near the shores around the airport and Seal Bay Armoury. Additionally, HMCS Quadra has a high liquefaction hazard. Overall, liquefaction increases near streams/rivers, deltas, sand spits, and areas of large fills.

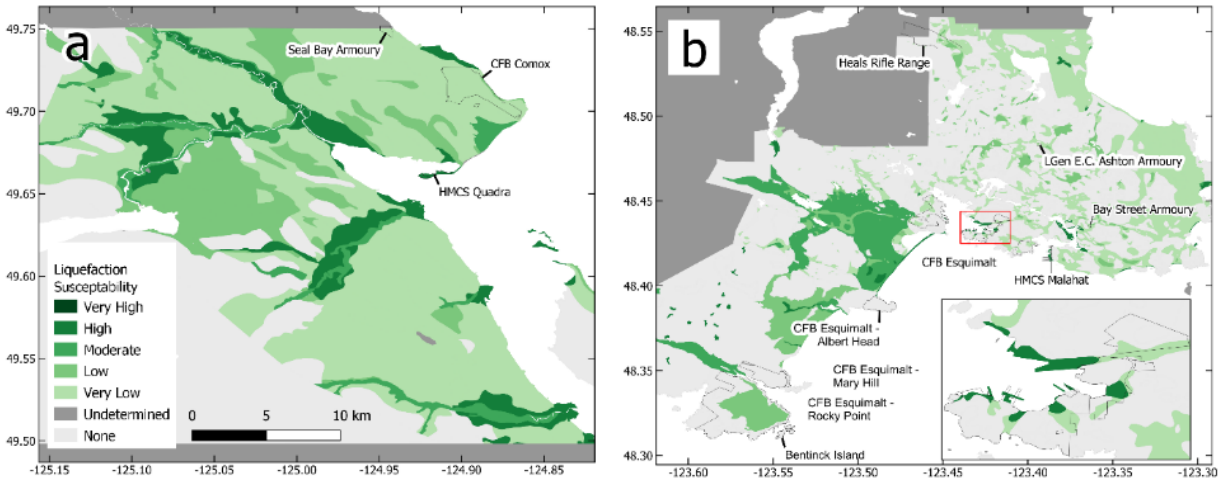

Figure 17: Liquefaction susceptibility of regions surrounding major DND bases. a) CFB Comox and area. b) CFB Esquimalt with inset of CFB Esquimalt Dockyard/Naden. Comox/Courtenay region is more susceptible to liquefaction overall due to the thicker quaternary sediment layer overlying bedrock (Blyth and Rutter), compared to the veneer sediments and bedrocks that dominate Victoria (Monahan).

The liquefaction probability is the likelihood that liquefaction will occur within each given geological unit during each scenario (Figure 18). The probability of liquefaction during each scenario is highly dependent on the susceptibility and whether the critical acceleration (HAZUS Table 4-12; FEMA 2020) is reached. This second factor means that the in-slab scenario event has minimal to no chance of creating liquefaction at CFB Esquimalt and CFB Comox. Meanwhile, the subduction scenario has the possibility of producing liquefaction at both sites (Figure 18). The liquefaction in Comox and Courtenay is confined mainly to the river valleys and deltas. These features are predominantly off base but strongly affect the downtown cores of both Courtenay and Cumberland. CFB Esquimalt has more direct impacts with the highest probabilities of liquefaction occurring near-shore within anthropogenic fills. As stated earlier, these fills underly docks and related infrastructure. Off-base around CFB Esquimalt, the probability of liquefaction is confined to low-lying areas and late quaternary sediments in Langford, Metchosin, and Colwood. The probabilities of liquefaction shown in Figure 18 are the probability that liquefaction will occurring within each given geological unit and not that the entire unit will experience liquefaction.

We did not factor in the absolute depth to the water table at each site during our calculation of the liquefaction probability and assumed a standard depth to the water table of 1.5 m (5 ft). We omitted this correction as the absolute value of water table depth is dependent on the tide (diurnal and monthly

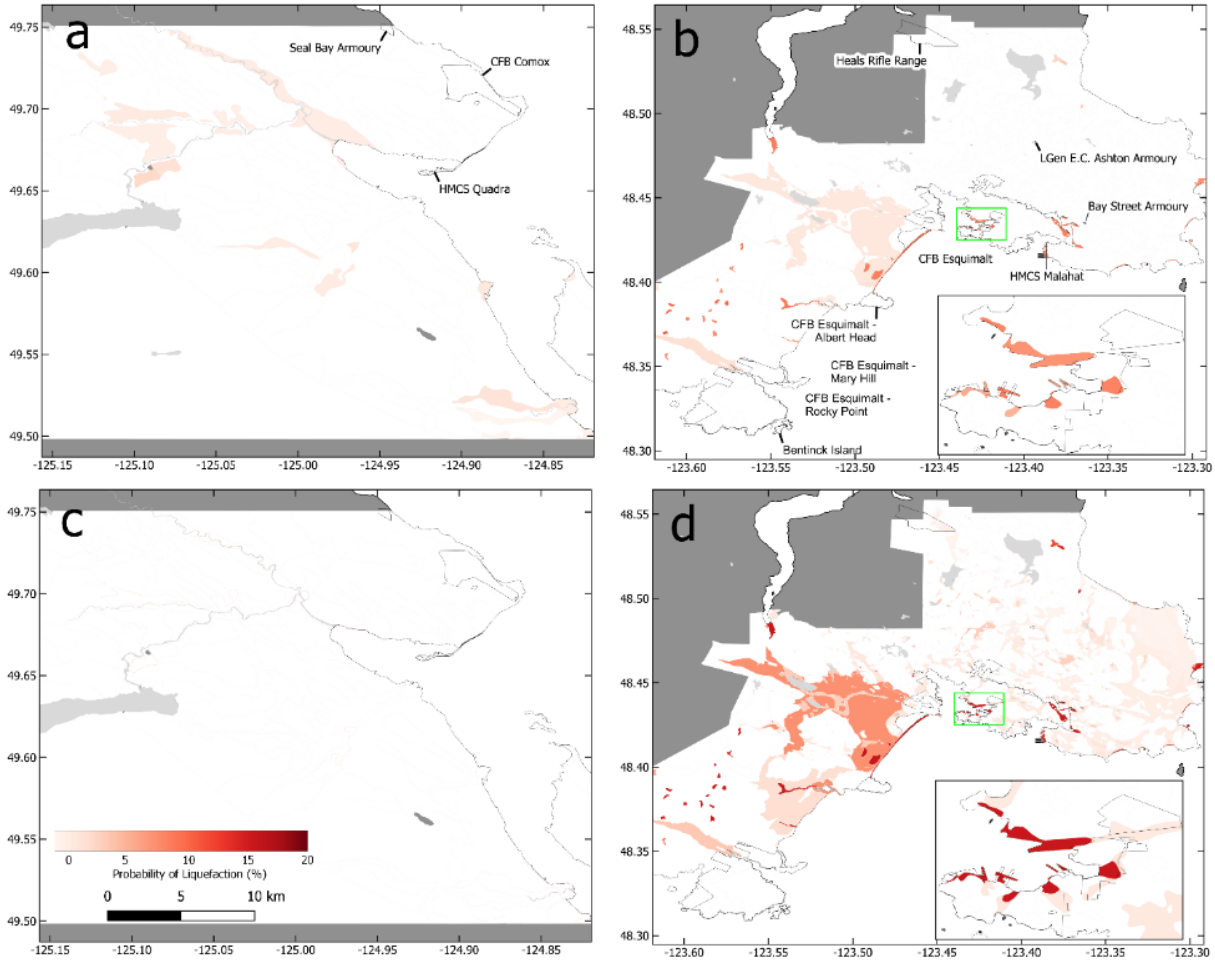

Figure 18: Liquefaction probability of regions surrounding major DND bases. a and b are for Subduction event, c and d are Crustal event. In-slab maps were not included as they scenario has no probability of producing liquefaction at either CFB Esquimalt or CFB Comox. Light grey are lakes and streams while dark grey are regions where probabilities were not determined. a) CFB Comox during subduction event – moderate probability near rivers/streams and minimal probabilities elsewhere. b) CFB Esquimalt with inset of CFB Esquimalt Dockyard. High (>10%) probability near low lying areas. For example, small ponds in Langford, areas around Esquimalt Lagoon and the fills near the shore in CFB Esquimalt Dockyard. c) Similar pattern as a, but reduced probabilities due to the lower PGA experienced. d) Similar pattern as b, with increased probabilities due to the increased PGA.

cycles) and seasonal (wet winter/spring or dry summer) conditions. Tidal variations affect near-shore geological units, with small (< 1 m) changes occurring on lunar cycle scales. Meanwhile, the seasonal changes can create >1 m changes in depth to the water table, especially in regions where the water table already extends above the surface (rivers, lakes, ponds). By ignoring this factor, we determined the generalized trend of liquefaction (Figure 19), but we are likely underestimating the liquefaction probability near these surface water features. If the water depth is known at a site, the probability can be corrected by multiplying the given probability with the correction factor K from equation 1.

$$K = \frac{1.40}{(0.07272 * d + 0.93)} \qquad \text{(Equation 1)}$$

where d is the water table depth in metres below the surface (Seed and Idriss, 1982; Seed et al., 1985; FEMA, 2020).

7.3 LANDSLIDE

Earthquakes are common triggers for landslides in areas with large slopes and appropriate geological conditions. Landslides are a significant earthquake-related hazard, accounting for approximately 5% of fatalities directly related to earthquakes worldwide between 1968 and 2008 (Marano et al., 2010). Landslides have been observed during several British Columbia and the Pacific Northwest earthquakes. For example, landslides were observed during the 1946 Vancouver Island crustal earthquake (Mathews, 1979), 2001 Nisqually in-slab earthquake (Creager et al., 2001), and the 2012 M7.8 Haida Gwaii earthquake (Barth et al., 2020). We looked at the impacts of potential landslides on and near CFB Comox and CFB Esquimalt. We separated the landslide hazard into two measures: landslide susceptibility and expected Peak Ground Deformation (PGD).

Susceptibility is the hazard without considering the ground shaking from a triggering earthquake. Areas are given a susceptibility value from 0 (None) to X (high susceptibility) based on the geological unit type, slope angle, and groundwater conditions (Ponti et al., 2008, and Wilson and Keefer, 1985). The susceptibility is an empirical measure of the cohesion and friction angle within a slope. When the critical acceleration (minimum PGA to trigger a failure) is reached the susceptibility directly determines the likelihood of a slope failure (Table 3).

PGD is the amount of permanent movement that has occurred due to the landslide. Given that a mass wasting event occurs the PGD is proportional to the PGA experienced by the body, the susceptibility category of the body, and the magnitude of the triggering earthquake. PGA and susceptibility determine the amount of PGD per waveform cycle, while the earthquake magnitude determines the number of cycles induced on the body by the seismic waves. The largest changes in PGD over distance are in the crustal scenario as the PGA decays quickly from the rupture plane.

Table 3: The likelihood of a landslide occurring in each susceptibility category given the critical acceleration is reached (Modified from FEMA, 2020; Table 4-17).

Susceptibility	**0 (None)**	**I**	**II**	**III**	**IV**	**V**	**VI**	**VII**	**VIII**	**IX**	**X**
Likelihood (%)	0	1	2	3	5	8	10	15	20	25	30

We collected our elevation data from the BC Lidar survey as a 1 m digital elevation model (DEM) (GeoBC, 2021) and resampled the DEM to 5 m resolution. We found that these DEM contains several notable features and artifacts that may produce errors in estimating landslide susceptibility. Most of the artifacts are edges of buildings that show up as sharp elevation changes and, therefore, steep slopes. Other features, such as retaining walls or fills next to roadways, show similar steep slopes, but these are realistic features. Though real, these steep slopes likely have lower than calculated landslide hazards as the slopes are engineered structures and not natural deposits. These features and artifacts are often easily picked out due to their unnaturally straight shape or that they stay parallel to the nearby roadways. The resampling to 5 m reduced the noise from the above artifacts without significantly impacting the slope values and resulting susceptibilities. To determine the possible landslide slope materials, we used the same geological data collected for the liquefaction section (Colwood – Fyles, 1960; CRD – Monahan et al., 2000, and Blyth and Rutter, 1993). We then calculated the landslide susceptibility from the slope and geological conditions using the methodology used in HAZUS (Wilson and Keefer, 1985; FEMA, 2020).

As discussed in the liquefaction section, we could not map the groundwater depth consistently over the regions. Therefore, we produced two sets of PGD and susceptibility. One group considered all slopes to have the groundwater level below the slope face (dry slope), and the second set assumed all slopes to be wet. Both cases will not be valid for the entire region at a single time as some riverbanks

may be wetter than higher slopes of hillsides in the same period. Still, together these will encapsulate the upper and lower bounds of susceptibility.

The Comox Valley area is dominated by three different areas of susceptibility (Figure 19). In the western limit the bedrock surfaced mountains have relatively low susceptibility (less than IV) in most cases, with some exceptions where the slope is very high (western edge of Figure 19a). The second type of susceptibility is the low susceptibilities covering most of the valley and Comox peninsula, including CFB Comox (Figure 19c). This is due to the overall low slope throughout the region. Lastly, the highest susceptibilities of the region are along the numerous steep banked rivers (Figure 19b). These have dry susceptibility values of VI to IX depending on the slope. The susceptibilities along the riverbanks increase to IX and X if the slopes are wet, which is possible due to their proximity to surface water.

In the CRD, there are a significant number of small areas of dry slope landslide susceptibilities of V (Figure 20a). These patches result from the Victoria Clays and the undulating character of the terrain, creating lower stability slopes. There are also areas of even higher susceptibility where these clays make steep slopes near the ocean shore. These slopes exist around Oak Bay, Cadboro Bay, Cordova Bay, Victoria Inner Harbour, and George waterway (Figure 20b). A third high susceptibility slope type in the CRD is the extremely steep (>30) bedrock slopes. These slopes are prevalent in the region's mountains and more prominent hills (e.g., Mount Finlayson, Mount Douglas/PKOLS, Metchosin Mountain, etc.) (Figure 20c).

The landslide hazards within the CFB Esquimalt locations are primarily made up of steep clays or steep bedrock susceptibility types (Figure 21). The Colwood site is a prime example of this (Figure 21a). Along the creek in the north of the area, the steeper slopes and clay soil result in moderate to very high landslide dry susceptibilities (V to IX). Meanwhile, the steep bedrock slopes produce moderate values (VI) on the south side of the Colwood base. The landslide susceptibility at CFB Esquimalt Dockyard is low to moderate (I-IV) due to the bedrock hillsides (Figure 21b). CFB Esquimalt also has the most obvious artifact in the dry dock along the north side of the base. The drydock shows susceptibilities up to IX, but this is unrealistic as the concrete structure making up the drydock likely will not fail in the same way as a natural slope with the same slope values. Rocky Point and Mary Hill show I-V susceptibilities (Figure 21c), like the Dockyard, resulting from steep bedrock hills in the area. More artifacts are visual here in the flat central area of the Rocky Point base. The moderate susceptibility values here are buildings and not evenly spaced slopes.

Due to the significant distance from the crustal and in-slab scenarios, the median PGA from both scenarios is too low to trigger any landslides in the Courtenay and Comox region. The critical acceleration (minimum trigger PGA) for a slope with a landslide susceptibility of X is 0.05 g. The maximum PGA for the crustal and in-slab scenarios around Comox is ~0.01 g. The subduction scenario produces significantly stronger shaking in the Comox area than the other two scenarios, PGA≈0.14g. This PGA is strong enough to trigger landslides in slopes with susceptibilities of IX and X. When we consider the slopes wet, we find a maximum PGD of ~3.2 m related to landslide activity. Alternatively, dry conditions only allow slopes to reach PGD of ~0.3 m (Electronic Supplement).

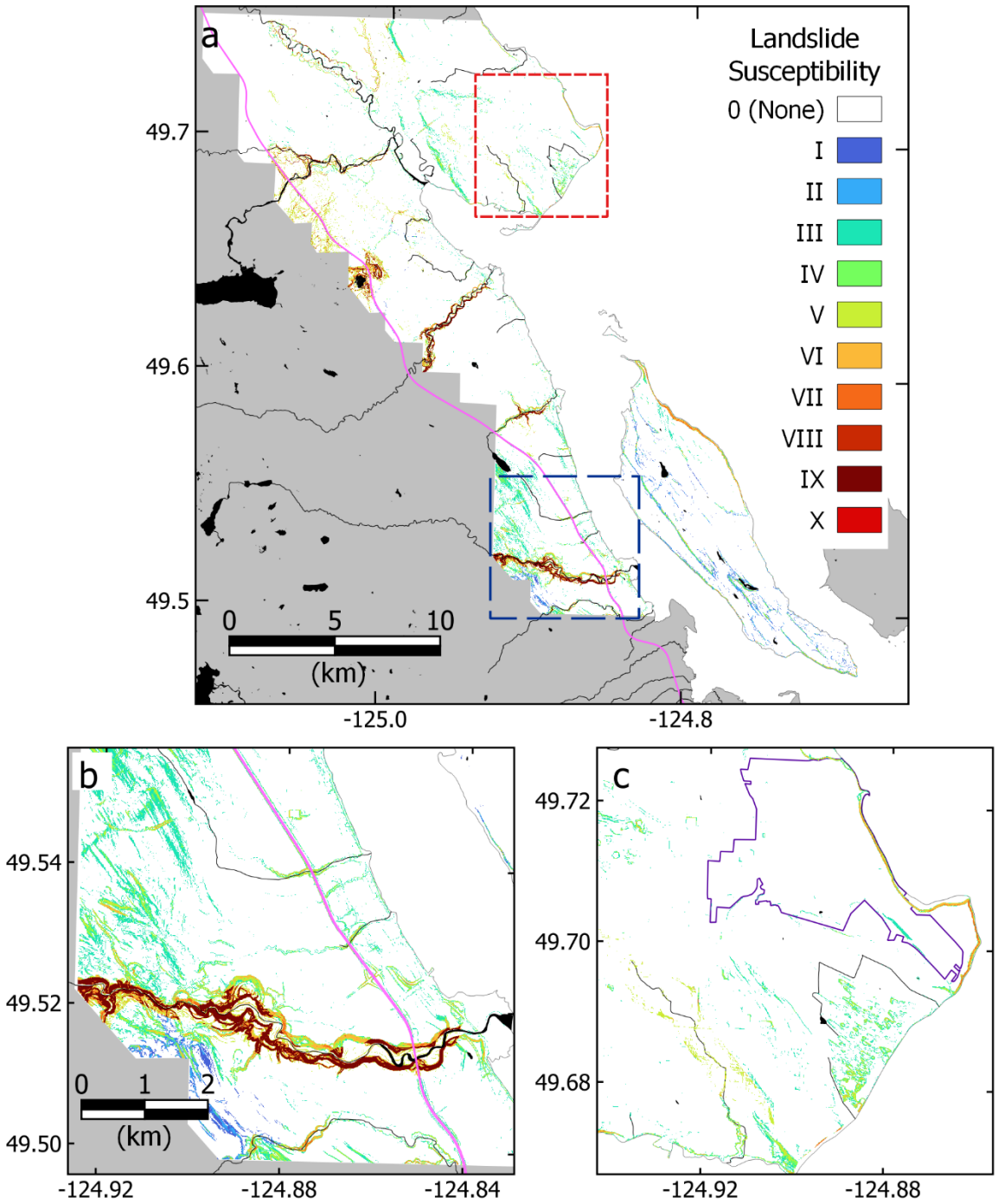

Figure 19: Dry Landslide susceptibility of Comox and Courtenay for dry slopes. a) Overview. No landslide susceptibility is shown in white while unmeasured areas are in grey, with fresh water in black and major roadways in pink. Boxes show b (blue) and c (red) images. B) Around Tsable River the moderate (VI) susceptibilities follow the riverbanks. The average landslide susceptibility values in this area increases towards the west due to the increasing number of hills. c) Around Cape Lazo the susceptibilities follow the steep bluffs along the shoreline on the eastern edge of CFB Comox (purple).

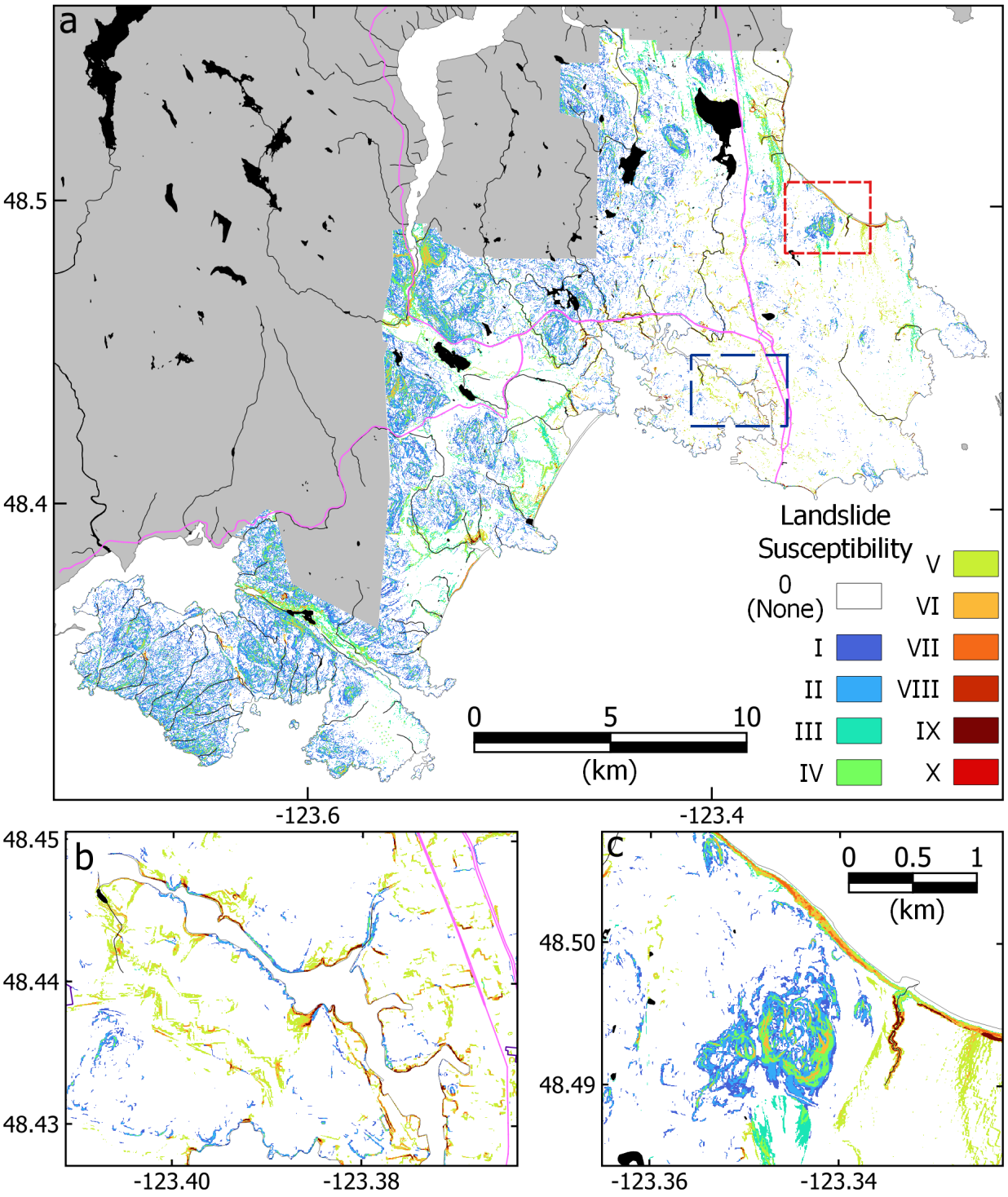

Figure 20: Landslide susceptibility of the CRD for dry slopes. A) Overview. No landslide susceptibility is shown in white while unmeasured areas are in grey. Fresh water streams and lakes in black and major roadways in pink. Relative to Comox there is significant small area susceptibilities through out the region. Boxes show b (blue) and c (red) images. b) Around George waterway the steeper banks showing landslide potential with the highest susceptibilities'(IX) where the Victoria clays meet the high slope. c) PKOLS (Mount Douglas) in Saanich showing the moderate susceptibility (IV-VI) of the rocky slopes. The nearby steep shoreline (up to 50°) consisting of sandy and clay like materials has high susceptibilities (VII-IX).

Unlike Comox and Courtenay, the CRD is located close to all three scenarios, and each scenario can trigger a landslide within the CRD. We found the in-slab scenario only produces landslides in clays and fills in both wet and dry conditions, and sandy soils if the groundwater level is high (Susceptibilities of IX and X). This is still significant as some slopes around Cadboro and Oak Bay, two popular public areas, fit into these categories and are estimated to produce a PGD of ~0.35 m in the wet scenario using the median PGA. With about twice the PGA in Victoria and nearly three times in Metchosin, the subduction interface event is expected to produce larger and more numerous landslides in the CRD. This scenario has the possibility of triggering slope failure on slopes with susceptibilities of VIII to X. On the extreme end of the landslide hazard for our three scenarios is the crustal, LRVDMF, scenario. This event occurring below the south of the CRD produces median PGA above 0.5g, strong enough to trigger landslides in all susceptible slopes except 0 and I. For high susceptibility slopes (X) PGD of up to 10 m can occur, with moderate slopes (IV-VI) experiencing PGD approaching 1 m. With such a strong effect, even if only a small percentage of the susceptible slopes fail, there will be significant number of landslides. Many of these will likely directly impact linear infrastructure throughout the region.

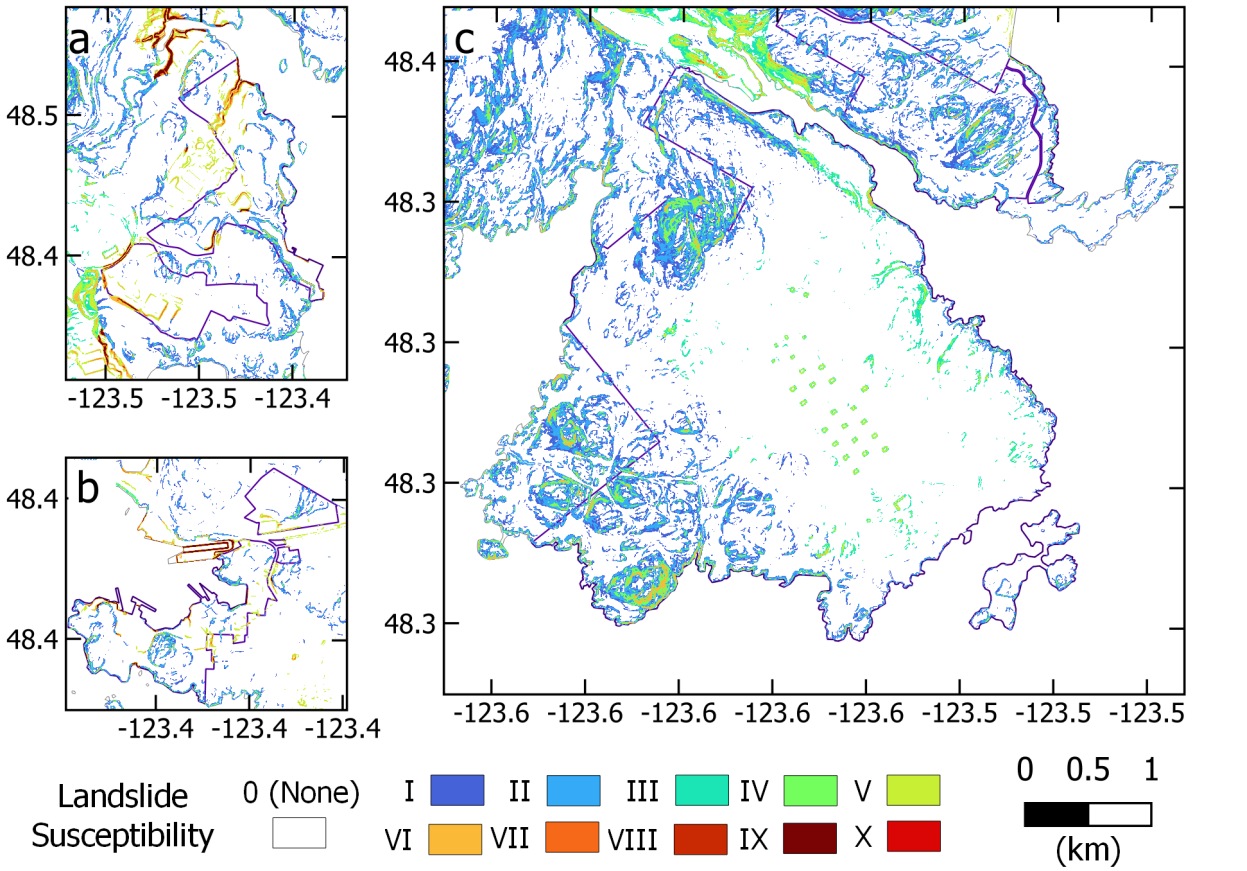

Figure 21: Landslide susceptibility of DND sites with outline of DND facilities shown in grey. A) Colwood and Belmont Park. b) Esquimalt Dockyard and Naden. c) Rocky Point and Mary Hill. Both a and b display moderate susceptibilities in lower slope areas of clays – such as the central part of Colwood and the Naden site, as well as very high hazards (IX) for very steep clays – North portion in Colwood and the Northwest tip of the Dockyard. Additionally, all three sites display values (VI and VII) around steep bedrock bluffs, with a and b showing through the sites and c showing these values near the water edge where the slopes are steepest. Artifacts from the dry docks in the dockyard show very high landslide susceptibility, but the likelihood is much lower as these are concrete structures and not natural slopes.

7.4 Surface Rupture

When an earthquake occurs, there is relative motion across the fault face. If the fault extends to the surface, the ground in this location will be offset. This motion can rupture building footings or linear infrastructure. The in-slab scenario is very deep (> 50 km) and will not rupture at the surface.

Morell et al. (2018) determined that the LRVF has had three surface rupturing earthquakes in the last 9 ka. If the LRV-DMF were to rupture, the transportation, communication, water, and gas infrastructure along the fault could be damaged. This damage to transportation links could increase response and recovery times in the densely populated Capital Regional District (CRD). Additionally, damage to the primary water source for the CRD (Sooke Lake, NW of Langford along the LRVF trace) could limit the amount of fresh water post-earthquake. Similarly, other communities on southern Vancouver Island could be cut off from Victoria if the rupture were to damage the highway and infrastructure.

It is possible for the Cascadia subduction event to have motion extend to the trench (Gao et al., 2018). In the case of a trench rupture, no structures will be directly affected as the rupture will occur beneath the seafloor. This rupture could damage submarine cables crossing the surface rupture (i.e., internet fibre optic cables), but likely the largest impact of a submarine surface rupture would be a tsunami.

7.5 Tsunami

A tsunami is a series of waves created when a volume of water is displaced in an ocean or large lake. This displacement can be created by earthquakes, landslides, meteor impacts, underwater explosions, or other disturbances. Only one of our scenarios, the megathrust earthquake, is likely to produce a tsunami directly. The modelling of a tsunami runup involves determining the uplift of the earthquake and modelling the water motion considering the near- and on-shore bathymetry and topography. The runup modelling is beyond this report, and instead, we have used the results from a recent study of a similar modelling of the Cascadia Megathrust (CRD, 2021, and Figure 22).

The CRD modelled inundations values use the higher high-water mean tide (HHWMT) as their ocean level datum. HHWMT is the average of 19 years of the highest tide level from each tidal day. Therefore, aside from the highest tide of each tidal day the ocean water level is likely to be below HHWMT. The CRD used HHWMT in their model to observe a realistic worst case scenario event and it should be kept in mind that the likely lower tide level will decrease the amount of inundation predicted by this model.

The CRD model determined that a maximum of 7 m and 6 m of runup is expected in Esquimalt and Victoria Harbours, respectively. These values are seen at the extreme ends of the harbours. At CFB Esquimalt, forty buildings at Colwood, 105 at Dockyard and Naden, and six at Rocky Point are expected to be within the inundation zone. Additionally, much of the dock structure is expected to be inundated.

Meanwhile, at CFB Comox, the runup is expected to be less than 1.5 m. Therefore, the inundation should be minimal except at HMCS Quadra and Nanoose Harbour. At HMCS Quadra, the elevation is <5 m; therefore, the runup will inundate the spit, including the access road. At Nanoose Harbour, the elevation quickly rises away from the shoreline; as such, the inundation will be confined to the dock structure and supporting buildings along the shoreline. In Greater Vancouver, the inundation is like that of CFB Comox, affecting only buildings on the near shore. In 2005, a joint study by the cities of Richmond and Delta (conducted by John Clague; City of Richmond, 2017) could find no evidence of tsunami deposits within the Fraser River delta and concluded that the tsunami threat to these communities is very small. Therefore, we consider the impact of a tsunami to be minimal at the DND bases in Greater Vancouver.

In addition to runup, drawdown, or drop in water level ahead of the tsunami, is also a significant hazard. Considerable drawdown can damage floating structures or boats, depending on the draft (depth of water required to float a boat), or create significant current while draining restricted waterways. AECOM (2013) determined Esquimalt Harbour will see up the most drawdown with up to 2 m, while Victoria Harbour may see ~1 m of drawdown. Drawdown is limited to a maximum of 1 m at other CFB Esquimalt sites and at CFB Comox. The drawdown creates significant currents at the harbour entrances. CRD (2021) found that current speeds up to 10 m/s are expected at the mouth of Esquimalt harbour, and ~8 m/s at the mouth of Victoria Harbour.

In addition to the amount of runup and drawdown, the timing of the tsunami will differ depending on location. For a scenario in the location that we have selected, the west coast of Vancouver Island should expect the first set of waves in 30 to 45 minutes. CFB Esquimalt should expect first waves arriving between 60 and 80 minutes, and CFB Comox arrival times will be on the scale of 2 to 3 hours (AECOM, 2013 and CRD 2021).

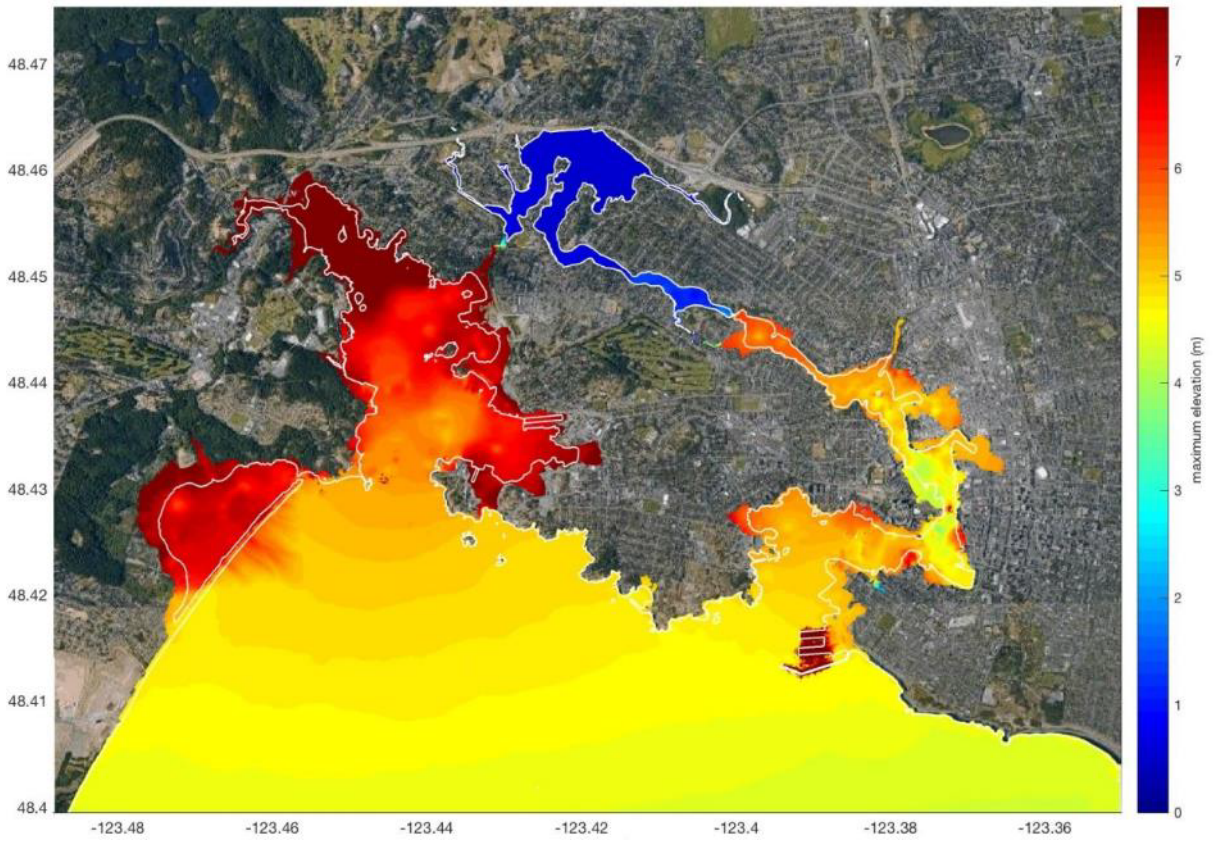

Figure 22: Calculated runup and inundation in Greater Victoria (CRD 2021; Figure 4-10). Maximum elevation is relative to the higher high-water mean tide (HHWMT).

7.6 FLOODING

Seismically induced flooding is a result of earthquake shaking damaging dams, dikes, or other water control measures, or lowering the land level such that it is no longer above water level. Estimating the expected damage to this infrastructure is beyond the scope of this report, but we can observe relative hazard from reports by authorities operating the above structures. The Province of British

Columbia determined that 25 Fraser valley dykes, and sea dykes in Richmond and Tsawwassen are vulnerable to damage (Vass, 2015). Damage to these dykes could lead to flooding of the nearby neighbourhood, but DND assets will likely see no direct effects in these scenarios.

Similarly, BC Hydro conducts reports on the seismic stability of their dams (BC Hydro, 2014, 2020). They have determined that their sites located on the Jordan River, Campbell River, and Bridge River systems are at the most risk. Damage to these systems can both cause significant damage to downstream communities and reduce the available power after an event. BC Hydro have been taking measures to reduce the hazard from these sites by reducing water levels, retrofitting these sites, or relocating communities in the downstream path (BC Hydro, 2020). We do not expect that any failure of the above structures will directly affect operationally important DND sites.

7.7 Fire

Seismic damage to power and gas distribution lines within or outside buildings can lead to gas leaks that can easily spark fires (e.g. Mousavi et al., 2008). In addition, damage to underground water systems, hydrants, and interior sprinkler systems can reduce the ability to suppress such fires. Fires can be a dominate post earthquake hazard depending on the earthquake and setting. For example, the 1994 Northridge earthquake had about 110 reported earthquake-related fires, with most put out before spreading to neighbouring buildings. Meanwhile, the 1995 Kobe earthquake caused damage to approximately five thousand buildings. The disparity between these two events is differences in building code, firefighting equipment, response, and access (Baker et al., 2012). The hazard to DND infrastructure from fire is beyond the scope of this report but is still a significant potential secondary hazard. Any analysis of the hazard related to fire follow earthquakes should follow the process outlined by Technical Council for Lifeline Earthquake Engineering (TCLEE, 2005). An example of this is an analysis of the fire hazard in Vancouver conducted by Scawthorn (2020) who examines the hazard, risk, and loss related to five scenarios – three of which are similar to our scenarios here.

7.8 Aftershocks

Aftershocks are smaller, but potentially closer, earthquakes in the region around the primary earthquake (mainshock) during the hours, days, months, or years following the mainshock. Aftershocks are most likely to occur within several fault lengths of the mainshock, increasing the hazard area significantly for large events. The number of aftershocks for a given earthquake is dependent on the earthquake rupture and tectonic setting. In general, the larger the mainshock, the larger the number of aftershocks and the larger the possible magnitudes. Although it is impossible to predict the exact number, magnitude, or location of aftershocks, we can forecast these properties using statistical estimations.

The current leading statistical model is the Epidemic Type Aftershock Sequence (ETAS) model (Ogata, 1989, 2011; Page et al., 2016). ETAS is a point-process model that can estimate the number of aftershocks expected at given magnitude ranges or a given time range. The USGS has produced an operational forecasting software using the ETAS model. We combined this software and the rupture characteristics to produce aftershock forecasts for each scenario (Tables S1-S3 in Suffix).

We expect the Cascadia event to produce over 31 000 aftershocks on the first day and 123 000 in the first year. Most of these events are M<5 and will not be felt in our study region. Meanwhile, our forecast also suggests it is more likely than not that an M>7 earthquake will occur within 24 hours of the mainshock. An aftershock of this magnitude can produce moderate shaking in the SWBC region and, depending on the motion of the aftershock, may create an additional tsunami. An aftershock of this size is also likely to further damage buildings and infrastructure and may ‘reset’ some aspects of response.

The close timing of these two significant events means that the aftershock's seismic hazard will occur when rescue and recovery operations are underway.

The in-slab event is the near opposite of the Cascadia scenario. We expected less than ten aftershocks from this event in the first year. This lack of aftershocks is typical for deep earthquakes; for example, the 2001 Nisqually event had just five recorded aftershocks (Creager and Xu, 2002). We expect these aftershocks to be M<5 and therefore may be felt in SWBC but are unlikely to cause any damage.

The aftershocks of the LRV-DMF scenario are likely to create the most significant relative hazard increase of the three scenarios. Though the aftershocks are less numerous and of lower magnitude than the Cascadia scenario, they are likely to occur close to the Capital Region along the LRV-DMF. If the M>5 aftershocks occur at shallow depths near a population centre, we expect a felt intensity of up to a Modified Mercalli Intensity of VI (strong). This hazard will be occurring to a region already in turmoil and cause additional damage to moderately damaged buildings – increasing the likelihood of collapses. It could also pose serious logistical challenges as buildings which that already been inspected may need to be re-inspected at a time when inspectors are limited.

8 CONCLUSION

We have considered three representative and realistic earthquakes of the primary hazard sources in southwestern British Columbia:

- The Cascadia Subduction event is an M_w 8.9 event that models rupture along the portion of the megathrust that is most primed for a future large earthquake.
- The M_w 6.8 in-slab event is similar to the 2001 Nisqually earthquake in both depth and magnitude but has been moved to a more threatening position for southern British Columbia.
- The crustal event is a moderate-sized M_w 6.4 earthquake occurring along the central portion of the Leech River Valley – Devil's Mountain Fault complex near Victoria.

Though these three earthquakes are considered representative of the hazard in the region, they may not be the exact events experienced and do not encapsulate all magnitudes, rupture behaviours, and locations of each earthquake type. Specifically, crustal, and in-slab sources can occur in many locations, including closer to DND assets than has been modelled here. Diverse sources will be required to fully explore the hazard of this region. Overall, the subduction event has the broadest effect on the region, causing widespread shaking and moderate hazard to each DND site we reviewed. Meanwhile, the in-slab and LRV-DMF earthquakes had more localized effects on Vancouver and Victoria, respectively.

In addition to the direct seismic hazard, we reviewed several secondary hazards. We found that the hazard related to aftershocks, tsunamis (in the Cascadia scenario), liquefaction, and landslide had the greatest impact on DND facilities and operations. However, we were unable to directly quantify the effects of flooding and fire on these facilities.

The hazard analysis is the first step of a mitigation and preparedness program. The next step is to analyze the risk, damage, and vulnerabilities created by the hazards discussed in this report. We will accomplish this next step by applying the DND and the general populations exposure (buildings, people, and infrastructure) to the hazards determined here. These results will be published in a companion document.

REFERENCES

AECOM, 2013, Modelling of Potential Tsunami Inundation Limits and Run-up, CRD, British Columbia, 45 p.

Allen, T. I., and D. J. Wald, 2007, Topographic Slope as a Proxy for Seismic Site-Conditions (VS30) and Amplification Around the Globe, Report 2007–1357, Open-File Report.

Audet, P., M. G. Bostock, N. I. Christensen, and S. M. Peacock, 2009, Seismic evidence for overpressured subducted oceanic crust and megathrust fault sealing, Nature, 457, no. 7225, 76–78, doi: 10.1038/nature07650.

Baker, G. B., P. C. R. Collier, A. K. Abu, and B. J. Houston, 2012, POST-EARTHQUAKE STRUCTURAL DESIGN FOR FIRE – A NEW ZEALAND PERSPECTIVE, International Conference on Structures in Fire, no. 7, 10.

Barrie, J. V., and H. G. Greene, 2018, The Devils Mountain Fault zone: An active Cascadia upper plate zone of deformation, Pacific Northwest of North America, Sedimentary Geology, 364, 228–241, doi: 10.1016/j.sedgeo.2017.12.018.

Barrie, J. V., B. Molloy, and K. Douglas, 2021, Preliminary assessment of active faulting in the Victoria/Esquimalt region of British Columbia, 8774, 8774 p.

Barth, S., M. Geertsema, A. R. Bevington, A. L. Bird, J. J. Clague, T. Millard, P. T. Bobrowsky, A. Hasler, and H. Liu, 2020, Landslide response to the 27 October 2012 earthquake (MW 7.8), southern Haida Gwaii, British Columbia, Canada, Landslides, 17, no. 3, 517–526, doi: 10.1007/s10346-019-01292-7.

BC Hydro, 2014, Keeping our system safe. Dam safety at BC Hydro, BC Hydro, British Columbia, 16 p.

BC Hydro, 2020, Seismic hazard & our dams: <https://www.bchydro.com/energy-in-bc/operations/dam-safety/seismic-hazards.html> (accessed February 6, 2021).

Blyth, H. E., and N. W. Rutter, 1993, surficial geology of the Sooke area of Southern Vancouver Island in British Columbia, BCGS, Open File, 1:50000.

Bostock, M. G., N. I. Christensen, and S. M. Peacock, 2019, Seismicity in Cascadia, Lithos, 332–333, 55–66, doi: 10.1016/j.lithos.2019.02.019.

City of Richmond, 2017, Tsunamis and Richmond: <https://www.richmond.ca/safety/prepare/city/hazards/tsunamis/tsunamistudy.htm> (accessed May 6, 2021).

Clague, J. J., and B. Ward, 2011, Pleistocene Glaciation of British Columbia, in *Developments in Quaternary Sciences*, Elsevier, 563–573.

CRD, 2021, Tsunami Modelling and Mapping Report, CRD, British Columbia, Capital Region Coastal Flood Inundation Mapping Project, 461 p.

Creager, K. et al., 2001, The Nisqually earthquake of 28 February 2001 - Preliminary Reconnaissance report, University of Washington, 32 p.

Creager, K., and Q. Xu, 2002, The 2001 Mw 6.8 Nisqually Earthquake and its Aftershocks, AGU Fall Meeting Abstracts.

Cubrinovski, M., M. Hughes, B. Bradley, J. Noonan, R. Hopkins, S. McNeill, and G. English, 2014, Performance of Horizontal Infrastructure in Christchurch City through the 2010-2011 Canterbury Earthquake Sequence, University of Canterbury, Canterbury, 139 p.

Earthquakes Canada, 2021, Frequently Asked Questions about Earthquakes (FAQ), Government: <https://earthquakescanada.nrcan.gc.ca/info-gen/faq-en.php#can_how_often> (accessed May 5, 2021).

FEMA, 2020, Hazus Earthquake Model Technical Manual, FEMA.

Fyles, J. G., 1960, Surficial Geology, Courtenay, Comox, Nelson, Nanaimo and Newcastle Districts, Vancouver Island, British Columbia, 32–1960, 32–1960 p.

Gao, D., K. Wang, T. L. Insua, M. Sypus, M. Riedel, and T. Sun, 2018, Defining megathrust tsunami source scenarios for northernmost Cascadia, Nat Hazards, 94, no. 1, 445–469, doi: 10.1007/s11069-018-3397-6.

GEM Foundation, 2020, The OpenQuake Engine, GEM Foundation, Pavia, Italy.

GeoBC, 2021, LidarBC - Open LiDAR Data Portal: <https://catalogue.data.gov.bc.ca/dataset/cc11fb58-4837-4d6f-b783-95173e040983> (accessed January 22, 2022).

Goldfinger, C., S. Galer, J. Beeson, T. Hamilton, B. Black, C. Romsos, J. Patton, C. H. Nelson, R. Hausmann, and A. Morey, 2017, The importance of site selection, sediment supply, and hydrodynamics: A case study of submarine paleoseismology on the northern Cascadia margin, Washington USA, Marine Geology, 384, 4–46, doi: 10.1016/j.margeo.2016.06.008.

Harrichhausen, N., K. D. Morell, C. Regalla, S. E. K. Bennett, L. J. Leonard, E. M. Lynch, and E. Nissen, 2021, Paleoseismic Trenching Reveals Late Quaternary Kinematics of the Leech River Fault: Implications for Forearc Strain Accumulation in Northern Cascadia, Bulletin of the Seismological Society of America, 111, no. 2, 1110–1138, doi: 10.1785/0120200204.

Highland, L. M., 2003, An Account of Preliminary Landslide Damage and Losses Resulting from the February 28, 2001, Nisqually, Washington, Earthquake, Report 2003–211, Open-File Report.

Hobbs, T. E., J. M. Journeay, and D. Rotheram, 2021, An earthquake scenario catalogue for Canada: a guide to using scenario hazard and risk results, 8806, 24 p.

Hodgson, E. A., 1946, British Columbia Earthquake, June 23, 1946, The Jounal of the Royal Astronomical Society of Canada, 40, 285–319.

Holzer, T. L., 1992, The Loma Prieta, California, Earthquake of October 17, 1989: Strong ground motion and ground failure, Report 1551, Reston, VA, Professional Paper.

Hunter, J. A. M., R. A. Burns, R. L. Good, and C. F. Pelletier, 1998, A compilation of shear wave velocities and borehole geophysics logs in unconsolidated sediments of the Fraser River Delta, British Columbia, 3622, 3622 p.

Hyndman, R. D., 2013, Downdip landward limit of Cascadia great earthquake rupture: CASCADIA GREAT EARTHQUAKE RUPTURE LIMIT, J. Geophys. Res. Solid Earth, 118, no. 10, 5530–5549, doi: 10.1002/jgrb.50390.

Hyndman, R. D., and K. Wang, 1993, Thermal constraints on the zone of major thrust earthquake failure: The Cascadia Subduction Zone, J. Geophys. Res., 98, no. B2, 2039–2060, doi: 10.1029/92JB02279.

Jefferies, M., and K. Been, 2015, Soil Liquefaction: A Critical State Approach, Second Edition, CRC Press.

Johnson, S. Y., S. V. Dadisman, D. C. Mosher, R. J. Blakely, and J. R. Childs, 2001, Active tectonics of the Devils Mountain Fault and related structures, northern Puget Lowland and eastern Strait of Juan de Fuca region, Pacific Northwest, Report 1643, Professional Paper.

Journeay, M., P. LeSueur, W. Chow, and C. L. Wagner, 2022, Physical exposure to natural hazards in Canada, 8892, 8892 p.

Kakoty, P., S. M. Dyaga, and C. Molina Hutt, 2021, Impacts of simulated M9 Cascadia Subduction Zone earthquakes considering amplifications due to the Georgia sedimentary basin on reinforced concrete shear wall buildings, Earthquake Engng Struct Dyn., 50, no. 1, 237–256, doi: 10.1002/eqe.3361.

Kao, H., K. Wang, R.-Y. Chen, I. Wada, J. He, and S. D. Malone, 2008, Identifying the Rupture Plane of the 2001 Nisqually, Washington, Earthquake, Bulletin of the Seismological Society of America, 98, no. 3, 1546–1558, doi: 10.1785/0120070160.

Kawasumi, H., 1968, General Report on the Niigata Earthquake of 1964, Tokyo Electrical Engineering College Press, Japan, 7 p.

Kirby, S., 1995, Interslab earthquakes and phase changes in subducting lithosphere, Rev. Geophys., 33, 287, doi: 10.1029/95RG00353.

Kolaj, M., J. Adams, and S. Halchuk, 2020, THE 6th GENERATION SEISMIC HAZARD MODEL OF CANADA, 12.

Li, G., Y. Liu, C. Regalla, and K. D. Morell, 2018, Seismicity Relocation and Fault Structure Near the Leech River Fault Zone, Southern Vancouver Island, J. Geophys. Res. Solid Earth, 123, no. 4, 2841–2855, doi: 10.1002/2017JB015021.

Li, S., K. Wang, Y. Wang, Y. Jiang, and S. E. Dosso, 2018, Geodetically Inferred Locking State of the Cascadia Megathrust Based on a Viscoelastic Earth Model, J. Geophys. Res. Solid Earth, 123, no. 9, 8056–8072, doi: 10.1029/2018JB015620.

Marano, K. D., D. J. Wald, and T. I. Allen, 2010, Global earthquake casualties due to secondary effects: a quantitative analysis for improving rapid loss analyses, Natural Hazards, 52, no. 2, 319–328, doi: 10.1007/s11069-009-9372-5.

Mathews, W. H., 1979, Landslides of central Vancouver Island and the 1946 earthquake, Bulletin of the Seismological Society of America, 69, no. 2, 445–450, doi: 10.1785/BSSA0690020445.

McCrory, P. A., J. L. Blair, F. Waldhauser, and D. H. Oppenheimer, 2012, Juan de Fuca slab geometry and its relation to Wadati-Benioff zone seismicity: JDF SLAB GEOMETRY AND WBZ SEISMICITY, J. Geophys. Res., 117, no. B9, doi: 10.1029/2012JB009407.

Merrill, R. J., M. G. Bostock, S. M. Peacock, A. J. Schaeffer, and S. W. Roecker, 2022, Complex Structure in the Nootka Fault Zone Revealed by Double-Difference Tomography and a New Earthquake Catalog, Geochem Geophys Geosyst, 23, no. 2, doi: 10.1029/2021GC010205.

Monahan, P. A., V. M. Levson, P. Henderson, and A. Sy, 2000, RELATIVE LIQUEFACTION AND AMPLIFICATION OF GROUND MOTION HAZARD MAPS OF GREATER VICTORIA, BCGS Geoscience Map, 2000, no. 3, 31.

Monahan, P. A., V. M. Levson, and B. Kerr, 2010, Liquefaction Hazard Map of Richmond, British Columbia, Liquefaction Hazard, Ministry of Energy, Mines and Petroleum Resources, British Columbia, Geoscience Map, Liquefaction Hazard, 1:20000.

Morell, K. D., C. Regalla, C. Amos, S. Bennett, L. Leonard, A. Graham, T. Reedy, V. Levson, and A. Telka, 2018, Holocene Surface Rupture History of an Active Forearc Fault Redefines Seismic Hazard in Southwestern British Columbia, Canada, Geophys. Res. Lett., 45, no. 21, doi: 10.1029/2018GL078711.

Morell, K. D., C. Regalla, L. J. Leonard, C. Amos, and V. Levson, 2017, Quaternary Rupture of a Crustal Fault beneath Victoria, British Columbia, Canada, GSAT, 4–10, doi: 10.1130/GSATG291A.1.

Motazedian, D., J. A. Hunter, A. Pugin, and H. Crow, 2011, Development of a Vs30 (NEHRP) map for the city of Ottawa, Ontario, Canada, Can. Geotech. J., 48, no. 3, 458–472, doi: 10.1139/T10-081.

Mousavi, S., A. Bagchi, and V. K. R. Kodur, 2008, Review of post-earthquake fire hazard to building structures, Can. J. Civ. Eng., 35, no. 7, 689–698, doi: 10.1139/L08-029.

Ogata, Y., 2011, Significant improvements of the space-time ETAS model for forecasting of accurate baseline seismicity, Earth Planet Sp, 63, no. 3, 217–229, doi: 10.5047/eps.2010.09.001.

Ogata, Y., 1989, Statistical model for standard seismicity and detection of anomalies by residual analysis, Tectonophysics, 169, nos. 1–3, 159–174, doi: 10.1016/0040-1951(89)90191-1.

Oleskevich, D. A., R. D. Hyndman, and K. Wang, 1999, The updip and downdip limits to great subduction earthquakes: Thermal and structural models of Cascadia, south Alaska, SW Japan, and Chile, J. Geophys. Res., 104, no. B7, 14965–14991, doi: 10.1029/1999JB900060.

Onur, T., 2001, SEISMIC RISK ASSESSMENT IN SOUTHWESTERN BRITISH COLUMBIA, University of British Columbia.

Pagani, M. et al., 2014, OpenQuake Engine: An Open Hazard (and Risk) Software for the Global Earthquake Model, Seismological Research Letters, 85, no. 3, 692–702, doi: 10.1785/0220130087.

Page, M. T., N. van der Elst, J. Hardebeck, K. Felzer, and A. J. Michael, 2016, Three Ingredients for Improved Global Aftershock Forecasts: Tectonic Region, Time-Dependent Catalog Incompleteness, and Intersequence Variability, Bulletin of the Seismological Society of America, 106, no. 5, 2290–2301, doi: 10.1785/0120160073.

Peacock, S. M., and K. Wang, 1999, Seismic Consequences of Warm Versus Cool Subduction Metamorphism: Examples from Southwest and Northeast Japan, Science, 286, no. 5441, 937–939, doi: 10.1126/science.286.5441.937.

Ponti, D. J., J. C. I. Tinsley, J. A. Treiman, and H. Seligson, 2008, Section 3: Deformation, in *The ShakeOut Scenario: U.S. Geological Survey Open-File Report 2008-1150 and California Geological Survey Preliminary Report 25*, Open-File Report 2008–1150.

Preston, L. A., K. C. Creager, R. S. Crosson, T. M. Brocher, and A. M. Trehu, 2003, Intraslab Earthquakes: Dehydration of the Cascadia Slab, Science, 302, no. 5648, 1197–1200, doi: 10.1126/science.1090751.

Rogers, G. C., and H. S. Hasegawa, 1978, A second look at the British Columbia earthquake of June 23, 1946, Bulletin of the Seismological Society of America, 68, no. 3, 653–676, doi: 10.1785/BSSA0680030653.

Saragoni, G. R., and P. Concha, 2004, Damaging Capacity of Cascadia Subduction Earthquakes Compared with Chilean Subduction, World Conference on Earthquake Engineering, 13, no. 76, 15.

Scawthorn, C., 2020, Fire following earthquake in the Vancouver region, 67, Institute for Catastrophic Loss Reduction, Toronto, Ontario, Canada, ICLR research paper series, 74 p.

Schmalzle, G. M., R. McCaffrey, and K. C. Creager, 2014, Central Cascadia subduction zone creep, Geochem. Geophys. Geosyst., 15, no. 4, 1515–1532, doi: 10.1002/2013GC005172.

Seed, H. B., and I. M. Idriss, 1982, Ground Motions and Soil Liquefaction During Earthquakes, 13, Ground Motions and Soil Liquefaction During Earthquakes, Oakland, Monograph Series.

Seed, H. B., K. Tokimatsu, L. F. Harder, and R. M. Chung, 1985, Influence of SPT Procedures in Soil Liquefaction Resistance Evaluations, Journal of Geotechnical Engineering, American Society of Civil Engineers, 111, no. 12, 1425–1445.

Statistics Canada, 2020, Gross domestic product (GDP) at basic prices, by census metropolitan area (CMA), Government of Canada.

Stirling, M., T. Goded, K. Berryman, and N. Litchfield, 2013, Selection of Earthquake Scaling Relationships for Seismic-Hazard Analysis, Bulletin of the Seismological Society of America, 103, no. 6, 2993–3011, doi: 10.1785/0120130052.

Taylor, G. W., P. Monahan, T. W. White, and C. Ventura, 2006, British Columbia school seismic mitigation program: Dominant influence of soil type on life safety of greater vancouver and lower mainland schools of British Columbia, 5, 2490–2500.

TCLEE, 2005, Fire Following Earthquake, Technical Council for Lifeline Earthquake Engineering, Reston.

Vass, G., 2015, Lower Mainland Dike Assessment, 3000427, Northwest Hydraulic Consultants Ltd, British Columbia, 233 p.

Wagner, C. L., J. M. Journeay, N. L. Hastings, and J. A. Prieto, 2015, Risk map atlas: maps from the earthquake risk study for the District of North Vancouver, 7816, 7816 p.

Wang, P.-L., S. E. Engelhart, K. Wang, A. D. Hawkes, B. P. Horton, A. R. Nelson, and R. C. Witter, 2013, Heterogeneous rupture in the great Cascadia earthquake of 1700 inferred from coastal subsidence estimates: GREAT CASCADIA EARTHQUAKE OF 1700, J. Geophys. Res. Solid Earth, 118, no. 5, 2460–2473, doi: 10.1002/jgrb.50101.

Wang, K., R. Wells, S. Mazzotti, R. D. Hyndman, and T. Sagiya, 2003, A revised dislocation model of interseismic deformation of the Cascadia subduction zone: REVISED DISLOCATION MODEL OF INTERSEISMIC DEFORMATION, J. Geophys. Res., 108, no. B1, doi: 10.1029/2001JB001227.

Wells, D. L., and K. J. Coppersmith, 1994, New Empirical Relationships among Magnitude, Rupture Length, Rupture Width, Rupture Area, and Surface Displacement, BSSA, 84, no. 4, 974–1002.

Wilson, R. C., and D. K. Keefer, 1985, Predicting Areal Limits of Earthquake Induced Landsliding, Evaluating Earthquake Hazards in the Los Angeles Region, 1360, USGS, U.S. Geological Survey Professional Paper, 317–493 p.

Worden, C. B., D. J. Wald, T. I. Allen, K. Lin, D. Garcia, and G. Cua, 2010, A Revised Ground-Motion and Intensity Interpolation Scheme for ShakeMap, Bulletin of the Seismological Society of America, 100, no. 6, 3083–3096, doi: 10.1785/0120100101.

Youd, T. L. et al., 2001, Liquefaction Resistance of Soils: Summary Report from the 1996 NCEER and 1998 NCEER/NSF Workshops on Evaluation of Liquefaction Resistance of Soils, J. Geotech. Geoenviron. Eng., 127, no. 10, 817–833, doi: 10.1061/(ASCE)1090-0241(2001)127:10(817).